

RSC Publishing PCCP

The absorption spectrum of H₂: CRDS measurements of the (2-0) band, review of the literature data and accurate ab initio line list up to 35000 cm⁻¹

Journal:	<i>Physical Chemistry Chemical Physics</i>
Manuscript ID:	CP-ART-09-2011-022912
Article Type:	Paper
Date Submitted by the Author:	13-Sep-2011
Complete List of Authors:	Campargue, Alain; Universite Joseph Fourier de Grenoble Kassi, Samir; Université Grenoble 1/CNRS, UMR5588 LIPhy Grenoble Pachucki, Krzysztof; Faculty of Physics, University of Warsaw Komasa, Jacek; Faculty of Chemistry, A. Mickiewicz University

SCHOLARONE™
Manuscripts

The absorption spectrum of H₂:
CRDS measurements of the (2-0) band,
review of the literature data
and
accurate *ab initio* line list up to 35000 cm⁻¹

Alain Campargue ^{a1}, Samir Kassi ^a, Krzysztof Pachucki ^b and Jacek Komasa ^c

^a *Université Grenoble 1/CNRS, UMR5588 LIPhy Grenoble, F-38041, France*

^b *Faculty of Physics, University of Warsaw, Hoża 69, 00-681 Warsaw, Poland*

^c *Faculty of Chemistry, A. Mickiewicz University, Grunwaldzka 6, 60-780 Poznan, Poland*

12th September 2011

Number of figures: 10

Number of Tables: 5

Running Head: *The absorption spectrum of H₂ up to 35000 cm⁻¹.*

Keywords: *hydrogen; H₂, quadrupole dipole, absorption spectroscopy, CRDS, spectroscopic database*

¹ Corresponding author: Alain. Campargue@ujf-grenoble.fr

Abstract

Five very weak transitions - $O(2)$, $O(3)$, $O(4)$, $O(5)$ and $Q(5)$ - of the first overtone band of H_2 are measured by very high sensitivity CW-Cavity Ring Down Spectroscopy (CRDS) between 6900 and 7920 cm^{-1} . The noise equivalent absorption of the recordings is on the order of $\alpha_{min} \approx 5 \times 10^{-11} cm^{-1}$ allowing for the detection of the $O(5)$ transition with an intensity of $1.1 \times 10^{-30} cm/molecule$, the smallest intensity value reported so far for a H_2 absorption line. A Galatry profile was used to reproduce the measured line shape and derive the line strengths. The pressure shift of the $O(2)$ and $O(3)$ lines was accurately determined from a series of recordings with pressure ranging between 10 and 700 Torr.

From an exhaustive review of the literature data, the list of H_2 absorption lines detected so far has been constructed. It includes a total 39 transitions ranging from the $S(0)$ pure rotational line near 354 cm^{-1} up to the $S(1)$ transition of the (5-0) band near 18908 cm^{-1} .

These experimental values are compared to a highly accurate theoretical line list constructed for pure H_2 at 296 K (0 - 35000 cm^{-1} , intensity cut off of $1 \times 10^{-34} cm/molecule$). The energy levels and transition moments were computed from high level quantum mechanics calculations. The overall agreement between the theoretical and experimental values is found very good for the line positions. Some deviations for the intensities of the high overtone bands ($V > 2$) are discussed in relation with possible pressure effects affecting the retrieved intensity values. We conclude that the hydrogen molecule is probably a unique case in rovibrational spectroscopy for which first principles theory can provide accurate spectroscopic parameters at the level of the performances of the state of the art experimental techniques.

1. INTRODUCTION

The absorption spectrum of hydrogen up to the visible range consists in vibrational bands of very weak electric quadrupole transitions. As a result of the high values of the vibrational frequency (about 4160 cm^{-1}) and of the rotational constant (about 60 cm^{-1} in the vibrational ground state), the spectrum is extremely sparse and only a few rovibrational absorption lines are observable for each vibrational band.

Long after the first detection of eight lines of the (2-0) and (3-0) bands by Herzberg [1], the H_2 transitions continue to be of interest. One of the reasons is that hydrogen and its isotopologues are test species for theoretical calculations and discrepancies have been found between some experimental results and quantum mechanics calculations, in particular for line intensities. Another strong motivation is that hydrogen absorption lines are of interest to probe planetary atmospheres in particular those of the outer planets [2-7], the weakness of H_2 transitions being an advantage to avoid or limit saturation effects. The quality of the H_2 spectral parameters (position, strength, pressure shift and line profile) has a direct impact on the modeling of the planetary atmospheres (see for instance Ref. [8]). This is why the question of the most accurate parameter values to be used is of importance. Indeed, the hydrogen molecule is probably a unique case in rovibrational spectroscopy, in the sense that the quality of *ab initio* calculations is so good that the choice between the theoretical values and the experimental determinations (when available) is worth to be considered.

In the last decades, the energy levels, dissociation energy and transition moments of H_2 , HD and D_2 have been calculated by different authors (see for instance Refs. [9-16]). Two of us have recently refined the energy values for all the 302 bound levels of H_2 in its electronic ground state ($X^1\Sigma_g^+$). The energy levels and transition moments were retrieved from high level quantum mechanics calculations which account for the nonadiabatic, relativistic, and quantum electrodynamics effects. The general theoretical framework is presented in Section 4 where the obtained theoretical results are used to construct the list of H_2 absorption lines at room temperature.

The main objective of the present study is to perform a systematic comparison of the laboratory measurements of H_2 absorption lines with the spectroscopic parameters obtained from these most advanced theoretical calculations, with a particular emphasis on intensity measurements. This comparison is based on (i) our new measurements of the first overtone band by high sensitivity CW-Cavity Ring Down Spectroscopy (CRDS) between 6900 and 7920 cm^{-1} , (ii) an exhaustive review of the literature data ranging from the pure rotational transitions up to the (5-0) $S(1)$ transition near 18907 cm^{-1} which is the highest energy

transition detected so far for H₂. The experimental values will be compared to our highly accurate theoretical line list constructed for H₂ at 296 K (0 - 35000 cm⁻¹, intensity cut off of 1×10⁻³⁴ cm/molecule).

After the description of the experimental setup (Section 2), we present in Section 3 the line profile analysis together with the derivation of the positions, intensities and pressure shifts of five (2-0) transitions recorded by CRDS. Section 4 is devoted to the calculation of the theoretical line list up to 35000 cm⁻¹. Finally, we present in Section 5 a review of the absorption transitions of H₂ reported in the literature data and a discussion about the agreement between experiment and theory.

2. EXPERIMENT DETAILS

The electric quadrupole transitions of H₂ form *O*, *Q* and *S* branches corresponding to $\Delta J = -2, 0$ and $+2$, respectively. The H₂ transitions were searched on the basis of their predicted line center calculated from the *ab initio* energy levels (see Section 4). The (2-0) band is centered at 8087 cm⁻¹. In the spectral range accessible with our set of seventy fibered distributed feedback (DFB) lasers (5850-7920 cm⁻¹), five transitions could be recorded, line by line, by high sensitivity CW-CRDS: *O*(*J*) with *J*=2-5 and *Q*(5). The strongest *O*(2) and *O*(3) lines were previously measured by Bragg et al. by Fourier Transform Spectroscopy (FTS) [17] while the weakest *O*(4), *O*(5) and *Q*(5) lines are newly reported (see **Table 1**).

The fibered DFB laser CW-CRDS spectrometer used for the recordings has been described in detail in Refs. [18-20]. The electro-polished stainless steel ring down cell (*l*= 1.42 m, inner diameter $\Phi = 11$ mm) was fitted by a pair of super-mirrors. A single set of high reflective mirrors was used for all the recordings. The reflectivity of the mirrors in the studied region corresponds to empty cell ring down times varying from 120 to 320 μ s. About 20 ring down events were averaged for each spectral data point. Each DFB laser diode has a typical tuning range of about 40 cm⁻¹ by temperature tuning from -10°C to 60°C. A 5 cm⁻¹ spectral section was scanned at a spectral resolution of about 2×10⁻³ cm⁻¹ (60 MHz) around each H₂ line. The achieved noise equivalent absorption α_{min} varied between 3×10⁻¹¹ and 10⁻¹⁰ cm⁻¹, depending on the wavelength.

The purity of the sample (purchased from Messer IC) was stated to be better than 99.99 %. The pressure measured by a capacitance gauge (MKS 1000 Torr full range with 0.1% stated accuracy) and the ring down cell temperature (*T*= 294 ±1 K) measured by a thermo sensor (TSic 501) were monitored during the recordings. Most of the spectra were

recorded with pressure values of 700.0 Torr except for the $O(2)$ and $O(3)$ lines for which a series of recordings was performed for pressure values ranging between 10 and 700 Torr.

Each 5 cm^{-1} wide piece of spectrum was calibrated independently on the basis of the wavelength values provided by a Fizeau type wavemeter (WSU-30 Highfinesse, 5 MHz resolution and 20 MHz accuracy). The absolute calibration provided by the wavemeter is better than $1 \times 10^{-3}\text{ cm}^{-1}$ (30 MHz). The drift of the wavemeter being very slow, relative wavenumber values are about 10 times more accurate for successive spectra recorded over a short period (one hour, for instance). When possible, the calibration was checked and refined using reference line positions of water [21] present as an impurity. For instance, a shift on the order of $2 \times 10^{-4}\text{ cm}^{-1}$ was found and corrected from a water line near the $O(2)$ transition.

3. LINE PROFILE ANALYSIS AND INTENSITIES DERIVATION

The profiles of hydrogen rovibrational transitions are well known to show a marked Dicke narrowing with increasing pressure values (see for instance Ref. [22]). The $O(2)$ and $O(3)$ lines were recorded at different pressures ranging from 10 to 700 Torr in order to study the pressure dependence of the profile and determine the pressure line shift. The comparison of the profiles at 50 to 700 Torr presented in **Fig. 1** illustrates the clear reduction of the line width and the significant position shift of the $O(2)$ line. The full width at half maximum (FWHM) decreases from 0.0659 cm^{-1} at 50 Torr to 0.0377 cm^{-1} at 700 Torr. Note that a reduction by more than a factor of four compared to the Doppler width was measured and interpreted for the (1-0) $Q(1)$ Raman transition at about 2 atm [23].

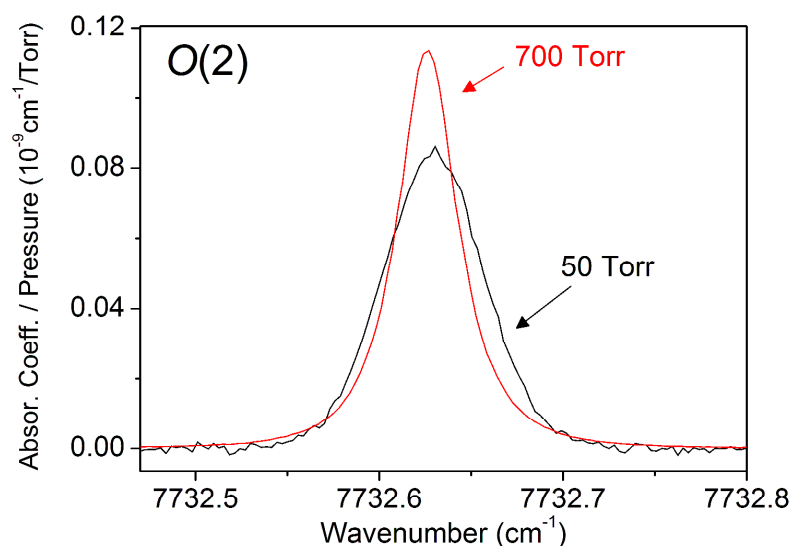


Fig.1

An interactive multi-line fitting program was used to reproduce the spectrum. The integrated absorption coefficient, A_{ν_0} ($\text{cm}^{-2}/\text{molecule}$), of a rovibrational transition centred at ν_0 (cm^{-1}), is related to the line intensity, S_{ν_0} ($\text{cm}/\text{molecule}$):

$$A_{\nu_0}(T) = \int_{\text{line}} \alpha_{\nu} d\nu = S_{\nu_0}(T)N \quad (1)$$

where: ν is the wavenumber in cm^{-1} , N is the H_2 concentration in $\text{molecule}/\text{cm}^3$ obtained from the measured pressure and temperature values: $N = P/kT$, $\alpha(\nu)$ is the absorption coefficient in cm^{-1} obtained from the cavity ring down time, τ (in s): $\alpha = \frac{1}{c} \left(\frac{1}{\tau} - \frac{1}{\tau_0} \right)$, where c is the light velocity and τ_0 is the ring-down time of the empty cavity.

In the line profile fitting, the DFB linewidth contribution (~ 2 MHz FWHM) was neglected as it represents about one thousandth of the Doppler broadening (~ 1.95 GHz FWHM). The FWHM of the Gaussian component was fixed to its theoretical value while the local baseline (assumed to be a linear function of the wavenumber), the line centre and the integrated absorbance were fitted.

The choice of the line shape used to reproduce the experimental profile is important as it may affect significantly the retrieved values of the line intensities. The fitting using a Voigt profile leads to a W shape residual which is the typical signature of the Dicke narrowing effect. A much better spectrum reproduction is obtained using a Galatry profile (**Fig. 2**). Some comparisons were also performed with a Rautian line shape, the latter leading however to *rms* values slightly larger (**Fig. 2**). More importantly, the values of the integrated absorption coefficient were found to deviate by up to 1.5 %, the Galatry values being systematically larger. This 1.5 % value is then our estimated uncertainty on the line intensities resulting from the choice of the line profile.

All the analyses presented below were performed using the Galatry profile. The results of the line profile fitting are illustrated in **Fig. 3** for the $O(3)$ and $Q(5)$ lines. In the case of the extremely weak $Q(5)$ line, the *rms* value of the residuals reaches the instrument noise level ($rms \sim 5 \times 10^{-11} \text{ cm}^{-1}$). This result was achieved taking into account a weak absorption line due to oxygen present as an impurity in our sample.

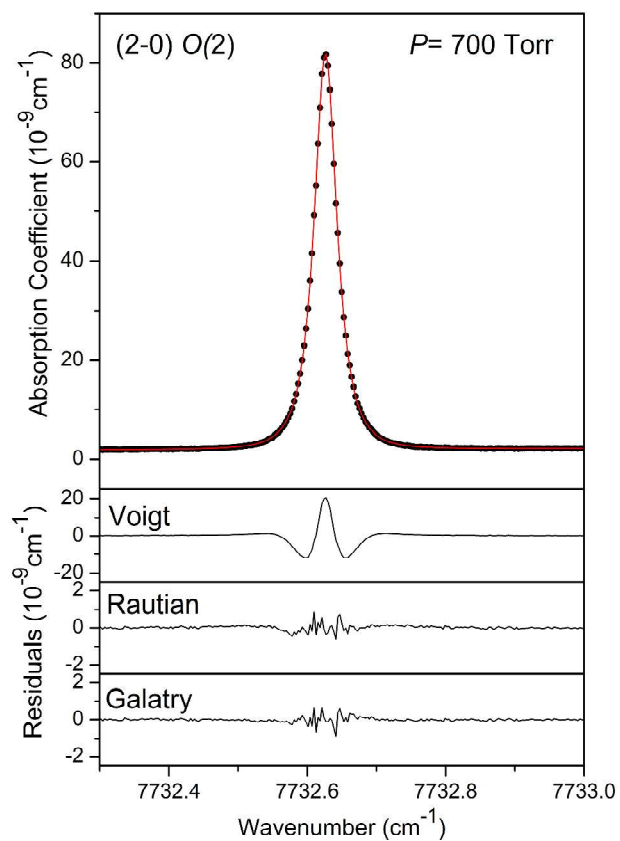


Fig. 2

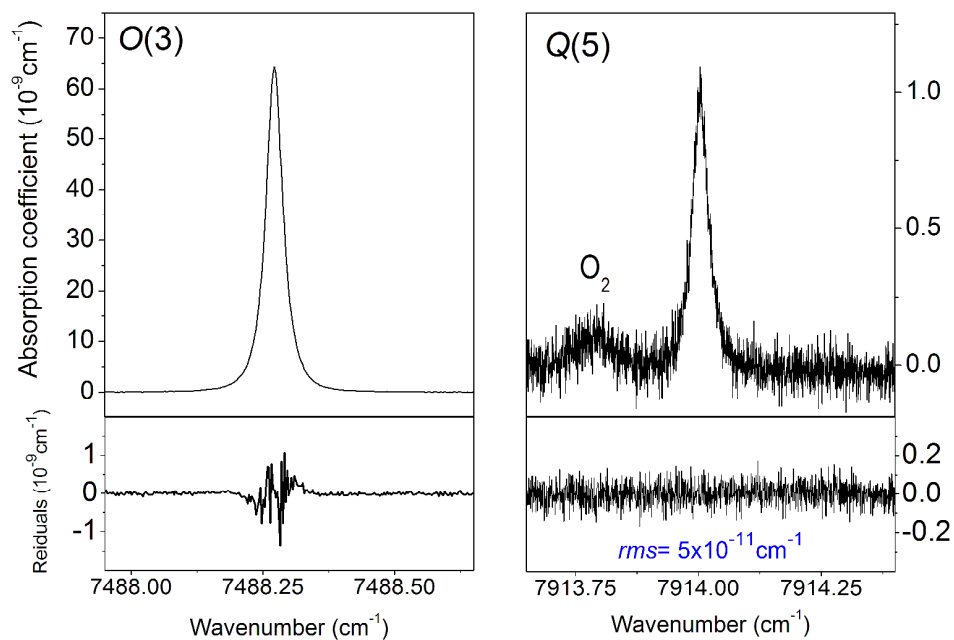


Fig. 3

The positions and intensities of the O(4), O(5) and Q(5) lines were retrieved from a single spectrum at 700 Torr. In order to increase the accuracy, the intensities of the O(2) and

$O(3)$ transitions were computed from the proportionality factor between the integrated absorption coefficient and the pressure values (Eq. 1). **Fig. 4** shows that the linear dependence is nearly perfect (regression coefficient of 0.99998 for both $O(2)$ and $O(3)$), yielding a statistical error bar on the order of 1‰ on the derived slope values.

The stability of our wavemeter over the duration of a series of recordings at different pressure values makes possible an accurate determination of the line shifts. **Fig. 4** shows the linear variation of the centre of the $O(2)$ and $O(3)$ lines with the pressure. Pressure shift values of $-3.62(14)\times 10^{-3}$ and $-3.33(16)\times 10^{-3}$ $\text{cm}^{-1}/\text{atm}$ at 294 K are obtained for $O(2)$ and $O(3)$, respectively. For an easier comparison with literature values, we have converted these values in $\text{cm}^{-1}/\text{amagat}$ which is the unit most frequently used for H_2 line shift (1 amagat is the molecular density corresponding to an ideal gas at 1 atm and 0°C). It leads to the values $-3.90(15)\times 10^{-3}$ and $-3.59(17)\times 10^{-3}$ $\text{cm}^{-1}/\text{amagat}$ for $O(2)$ and $O(3)$, respectively. The error bar is a combined effect of the wavemeter fluctuations and of the uncertainty on the line centre determination. The only previous experimental values of these line shifts are the very rough estimates given in Ref. [13]: $-5(5)$ and $-5(10)\times 10^{-3}$ $\text{cm}^{-1}/\text{amagat}$, respectively. Our values seem to be the most accurate determination of pressure shifts of H_2 transitions available in the literature.

Kelly and Bragg have used a semi classical approach to predict the line shifts as a function of the upper rovibrational transitions [24]. For the (2-0) $O(2)$ and $O(3)$ lines, they obtained -3.6×10^{-3} and -3.3×10^{-3} $\text{cm}^{-1}/\text{amagat}$, respectively, in very good agreement with our experimental values.

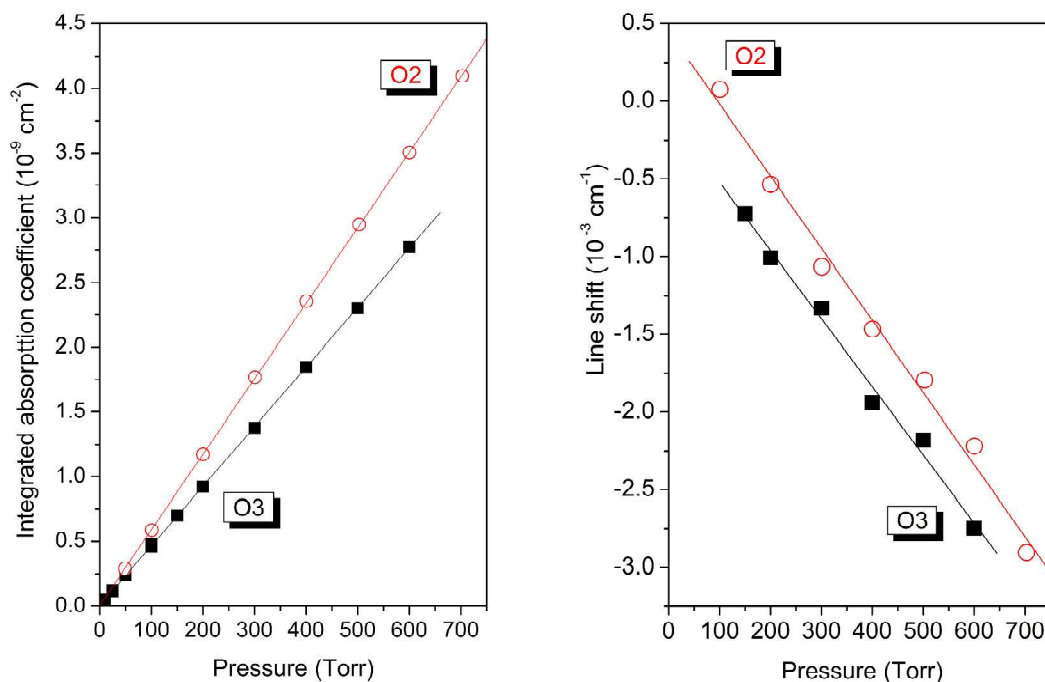


Fig. 4

The retrieved position and intensity values are included in **Table 1**. The intensities vary from 1.01×10^{-30} to 1.79×10^{-28} cm/molecule. The weakest lines are the $O(5)$ and $Q(5)$ transitions starting from the $J=5$ level at 1740.19 cm^{-1} . Let's emphasize that at 296 K, the fraction of H_2 molecules in the $J=5$ level is only 9.12×10^{-4} . With the $S(5)$ pure rotational transition detected in the far infrared [25], the $O(5)$ and $Q(5)$ (2-0) transitions are apparently the H_2 transitions with highest rotational excitation detected so far by absorption spectroscopy at room temperature. The temperature values of our experiments being 294 K while a reference temperature of 296 K is usually adopted, we have computed the corresponding intensity values at 296 K. All our intensity values are increased at 296 K, the variation reaching 5 % for the $O(5)$ and $Q(5)$ lines.

In the next section, we present the construction of the theoretical line list which will be used for comparison with experimental data.

4. THE THEORETICAL LINE LIST FOR H_2 UP TO 35000 cm^{-1}

Accurate ab initio calculations of the energy levels and quadrupole transition moments

Up to recently, the most accurate and comprehensive theoretical data for both the energy levels and the quadrupole transition moments of H_2 were computed by Wolniewicz

[10-14]. Since he has not given any uncertainties on his results, the comparison with those data is one-sided. Wolniewicz's methodology differs from ours in a few aspects. For instance, in our approach the nonadiabatic effects are included in the interaction potential and in the R -dependent effective nuclear reduced masses. Then, from a single set of interaction potentials all the energy levels are obtained by solving the one-dimensional Schrodinger equation. In contrast, Wolniewicz applied a separate nonadiabatic correction to every individual rovibrational level. In the 1995 paper [10] Wolniewicz expressed the rovibrational energies by coefficients of certain power series in $J(J+1)$ and limited himself to levels with $J \leq 10$. The Born-Oppenheimer potential he used was of the state-of-the-art quality at that time but today it turns out to be several orders of magnitude less accurate than that currently available [16]. Also the incomplete quantum electrodynamics (QED) corrections limited the accuracy of Wolniewicz's results.

Our *ab initio* computational approach is based on the expansion of the bound state energy in a series of powers of the fine structure constant, α :

$$E(\alpha) = E_{NR} + \alpha^2 E_{REL} + \alpha^3 E_{QED} + \alpha^4 E_{NQED} + \dots \quad (2)$$

Subsequent terms of this expansion represent the nonrelativistic, the relativistic, the leading QED, and higher order QED contributions to the total energy. In the frame of the nonrelativistic expansion of quantum electrodynamics theory (NRQED) [26,27], each contribution can be evaluated as an expectation value of a certain effective Hamiltonian with the nonrelativistic wave function. These effective Hamiltonians are known for all terms up to α^4 . However, calculations of the last α^4 term are quite complicated and so far have been performed accurately only for the helium atom. Calculations of the lower order terms for the hydrogen molecule go as follows. The nonrelativistic wave function is a solution of the Schrödinger equation $H\Psi = E\Psi$. To solve this equation we at first assume the adiabatic approximation in which the total wave function is represented by a product of the electronic and the nuclear wave functions $\Psi(\mathbf{r}, \mathbf{R}) = \varphi(\mathbf{r}; \mathbf{R})\chi(\mathbf{R})$. The electronic wave function is an eigenfunction of the electronic (clamped nuclei) Hamiltonian H_{el} , whereas the nuclear function $\chi(\mathbf{R}) = Y(\vartheta, \varphi)\chi_J(R)/R$, after separation of the angular variables in the spherical harmonic $Y(\vartheta, \varphi)$, is the solution to the radial nuclear Schrödinger equation. Adiabatic and nonadiabatic corrections are calculated using nonadiabatic perturbation theory (NAPT) [28]. With accuracy of $O(m_e/M)^2$ the rovibrational energies can be obtained from the so called nonadiabatic nuclear equation:

$$\left[-\frac{1}{R^2} \frac{\partial}{\partial R} \frac{H^2}{2\mu_{\parallel}(R)} \frac{\partial}{\partial R} + \frac{J(J+1)}{2\mu_{\perp}(R)R^2} + V(R) \right] \chi_J(R) = E_{NR} \chi_J(R). \quad (3)$$

Here $V(R) = E_{BO}(R) + E_{AD}(R) + E_{NA}(R)$ is a nonadiabatic interaction potential composed of the Born-Oppenheimer potential augmented by adiabatic and nonadiabatic corrections. The two functions $\mu_{\parallel}(R)$ and $\mu_{\perp}(R)$ are the R -dependent effective nuclear reduced masses. To take into account the relativistic and QED effects we extend the effective potential by further corrections:

$$V(R) = E_{BO}(R) + E_{AD}(R) + E_{NA}(R) + E_{REL}(R) + E_{QED}(R) + E_{HQED}(R) + E_{FS}(R). \quad (4)$$

These corrections represent the electronic expectation value of the Breit-Pauli Hamiltonian, E_{REL} , the leading E_{QED} and the higher order (E_{HQED}) QED effects, as well as the effect of the finite size of the nuclei, E_{FS} .

The Born-Oppenheimer (BO) potential is obtained by solving the clamped nuclei equation using variational approach. The electronic wave function is represented as a linear combination of properly symmetrized two-electron basis functions, such as the James-Coolidge for short internuclear distances and the generalized Heitler-London for large distances. The achieved relative accuracy in BO energy is about 10^{-15} , which significantly exceeds that of the previous best calculations by Cencek [29] and by Sims and Hagstrom [30]. For evaluation of all the corrections we applied exponentially correlated Gaussian (ECG) functions [31] with carefully optimized nonlinear parameters. This includes the computation of the quadrupole moment function:

$$Q(R) = \frac{R^2}{2} - \frac{1}{2} \left\langle \varphi \left| \sum_i 3z_i^2 - r_i^2 \right| \varphi \right\rangle \quad (5)$$

needed for the quadrupole transition moments and the line intensities. At present, we neglect the contribution to the intensity coming from the magnetic dipole transitions [32] because its significance in the intensity is below the experimental uncertainty. More elaborated description of the methodology can be found in Refs. [33-36]. Ref. [36] contains the complete list of the dissociation energy of the 302 bound levels of H_2 .

Line list construction

On the basis of these accurate theoretical calculations, the complete list of H_2 absorption transitions up to 35000 cm^{-1} was constructed. The spectrum consists of a series of ($V'=0-12$, $V''=0$) vibrational bands corresponding to the excitation of the (V', J') upper rovibrational levels from the ($V''=0, J''$) ground levels. Following the electric quadrupole selection rules,

the rotational structure of each vibrational band exhibits O ($\Delta J = -2$), Q ($\Delta J = 0$) and S ($\Delta J = +2$) branches. The transition frequencies (in cm^{-1}) were obtained as the difference of the calculated energy levels of Ref. [36]. Each frequency value is accompanied by its individual uncertainty which increases gradually with the energy from a few 10^{-5} cm^{-1} for the pure rotational transitions up to $5 \times 10^{-3} \text{ cm}^{-1}$ near 35000 cm^{-1} .

Following the conventions adopted in the HITRAN database [21], the line intensities were calculated at a reference temperature of 296 K and the intensity values are expressed in $\text{cm}/\text{molecule}$ for pure H_2 . The intensity cut off was fixed to a very small value of $1 \times 10^{-34} \text{ cm}/\text{molecule}$. We estimate the relative uncertainty on the line intensities to be below 0.1%.

The line intensities, S_{v_0} ($\text{cm}/\text{molecule}$), were computed from the quadrupole transition moment, $\langle V'J' | Q | V''J'' \rangle$, using the following expression [9, 37]:

$$N_0 S_{v_0} = 2.208 \times 10^{-15} \nu^3 P_J C_J \langle V'J' | Q | V''J'' \rangle^2 \quad (6)$$

where: ν is the calculated wavenumber (cm^{-1}), N_0 is the Loschmidt's number ($2.687 \times 10^{19} \text{ molecules}/\text{cm}^3$), $\langle V'J' | Q | V''J'' \rangle$ is expressed in Debye \times angstrom ($10^{-8} \text{ D}\cdot\text{cm}$) (1 a.u. corresponds to $1.345 \times 10^{-8} \text{ D}\cdot\text{cm}$), P_J is the fraction of molecules in the J rotational level at the considered temperature. P_J was calculated from $P_J = g_J (2J + 1) \exp(-E_J / kT) / Z(T)$ where $g_J = 1, 3$ for J even or odd, E_J is the calculated value of the ground state rotational level and Z the partition function: $Z(T) = \sum_J g_J (2J + 1) \exp(-E_J / kT)$. C_J is the appropriate Clebsch-Gordan coefficient [9, 10]:

$$C_J = \frac{3(J+1)(J+2)}{2(2J+1)(2J+3)} \text{ for a } S(J) \text{ transition } (J' = J'' + 2), \quad (7)$$

$$C_J = \frac{J(J+1)}{(2J-1)(2J+3)} \text{ for a } Q(J) \text{ transition } (J' = J''), \quad (8)$$

$$\text{and } C_J = \frac{3J(J-1)}{2(2J-1)(2J+1)} \text{ for a } O(J) \text{ transition } (J' = J'' - 2) \quad (9)$$

In total, the line list consists in 175 transitions belonging to the (V -0) vibrational bands with $V \leq 12$. **Fig. 5** shows an overview of the obtained line list. The strongest line of each (V -0) band is the $S(1)$ transition whose intensity is decreasing from $3.2 \times 10^{-26} \text{ cm}/\text{molecule}$ for the (1-0) fundamental to $2.5 \times 10^{-33} \text{ cm}/\text{molecule}$ for the (12-0) band. We checked that the line intensities of the (V -1) hot bands are all below the chosen intensity cut off. The 25 transitions of the first overtone band presented in **Table 2** are extracted from the global line list provided as Supplementary Material. The global line list includes the calculated values of the transition

frequencies and intensities, the corresponding lower state energy and Boltzmann factor, together with the quadrupole transition moment (in atomic unit).

In the next section, we review the laboratory observations of H_2 absorption transitions available in the literature with particular emphasis on intensity measurements. The experimental values including our CRDS measurements of the (2-0) band will be compared to our calculated line list in Section 6.

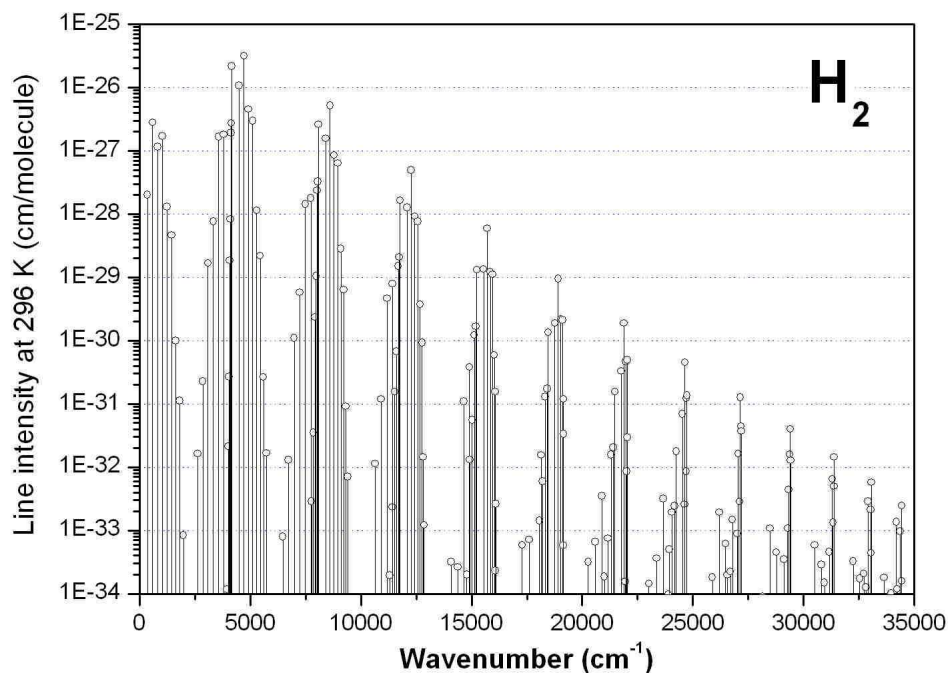


Fig. 5

5. A REVIEW OF THE LABORATORY MEASUREMENTS OF H_2 ABSORPTION TRANSITIONS

Due to their importance in astrophysics, considerable experimental efforts have been developed to measure the very weak quadrupole transitions of H_2 . We have collected in **Table 3** the spectroscopic parameters of the H_2 absorption lines available in the literature together with our CRDS measurements. This table is limited to laboratory data obtained by absorption [17, 25, 37-48] because they generally provide the best accuracy and we want to discuss the absorption line strengths. Nevertheless, we mention that additional line positions or energy levels were obtained from Raman spectra [22,49-55], electric field induced absorption spectroscopy [52,56] or astronomical observations [57]. For instance, (i) the Raman investigations by Veirs and Rosenblatt of the (0-0), (1-0) and (2-0) bands (estimated uncertainty of $\pm 0.03 \text{ cm}^{-1}$) include the O branch of the (1-0) band [50], (ii) Jennings et al.

reported high J line positions up to $J=7$ for the (0-0) and (1-0) Raman bands measured in diffusion flames [51] and (iii) Germann et al. used CARS spectroscopy to measure $Q_v(J)$ transition energies for $V=0-4$, $J=0-18$ with an accuracy of 0.05 cm^{-1} [53] and (iv) Knacke and Young detected the $S(8)$ and $S(12)$ - $S(15)$ pure rotational lines in Orion (uncertainty of $\pm 1\text{ cm}^{-1}$) [57]. Emission spectroscopy of the Lyman and Werner bands in the vacuum ultraviolet [58,59] give access to practically all the bound energy levels of H_2 . In particular, Dabrowski could determine with accuracy on the order of 0.1 cm^{-1} , most of the 302 bound energy levels of H_2 up to 1 cm^{-1} below the dissociation energy ($D_0=3618.0696(11)\text{ cm}^{-1}$ [36]) [59]. Due to their limited accuracy, some results obtained by absorption (e.g. from Refs [1, 60]) are not included in **Table 3**.

Following the pioneer works, most of the measurements were performed in the 70s and 80s using long base multipass cells, in particular those located at Kitt Peak and at Denison University (Granville, Ohio) [61]. The most extensive study is due to Bragg, Brault and Smith who reported a total of 26 positions and 22 intensities values for transitions of the (1-0), (2-0), (3-0) and (4-0) bands studied with the Kitt Peak solar Fourier transform spectrometer [17]. These measurements were performed at room temperature with H_2 pressures ranging between 0.8 and 2.8 atm. The absorption pathlength was 434 m. It is worth mentioning also the high quality results reported by Fink, Wiggins and Rank in 1965 [40], about twenty years before the work of Bragg et al.. These authors measured nine lines of the (1-0) and (2-0) bands from spectra recorded with an "échelle type" grating spectrograph associated with a 44-meter White cell (absorption path length up to 1.4 km).

A few transitions could be detected by combining multipass cells with laser sources instead of wide spectrum light sources:

- the $S(0)$ pure rotational line near 587 cm^{-1} was measured by Reuter and Sirota with a lead-salt diode laser ($l=52\text{ m}$, $0.3 < P < 1.3\text{ atm}$) [43]
- a lead-salt diode laser was also used by Reid and McKellar to measure the $S(3)$ line near 1035 cm^{-1} ($l=300\text{ m}$, $P < 700\text{ Torr}$) [38]
- the $S(1)$ line of the same (2-0) band near 8604 cm^{-1} was measured by Chackerian and Giver with an Optical Parametric Oscillator (OPO) pumped by a pulsed Nd:YAG laser ($l=907\text{ m}$, $2.4 < P < 3.2\text{ atm}$) [37,44]
- Finally, Ferguson et al. investigated the (4-0) $S(0)$ and $S(1)$ lines and the (5-0) $S(1)$ line in the visible range by using a high resolution ring dye laser [46]. Absorption pathlengths up to 5.984 km were achieved with 272 passes in a 22m-base multi-pass cell ($P < 4\text{ atm}$) located at Denison University

Prior to our CRDS study, this (5-0) $S(1)$ transition near 530 nm was the weakest line detected so far for H_2 (measured intensity of 6.5×10^{-30} cm/molecule [45]). Indeed, the combination of laser sources with high finesse cavities allows to further increase the sensitivity. These cavity enhanced absorption techniques (CW-CRDS, CEAS, OF-CEAS, ICOS...) have the advantages of requiring small sample volume (about 110 cm³ in our case) which in turn reduces the hazardous risks in the case of hydrogen and allows studying minor isotopologues at reduced expenses [42,62]. Because of their performances in terms of sensitivity and spectral resolution (in particular when CW lasers are used), these laser techniques are particularly well suited to study the H_2 line profiles which are not yet fully understood and have direct impact on the retrieved intensity values (see Section 3). Nevertheless, the performances of the cavity enhanced techniques depend on the availability of laser sources and of very high reflective mirrors at the required frequencies. Apart the present work by CRDS, only two H_2 studies based on high finesse cavities were reported so far:

- the $Q(1)$ line of the (2-0) band near 8075 cm^{-1} was studied by Gupta et al. using Integrated Cavity Output Spectroscopy (ICOS) with a single mode DFB diode laser ($P < 900$ Torr) [42]
- the line strengths of seven transitions of the (3-0) band were determined by Robie and Hodges by pulsed-CRDS using a dye laser as light source ($0.1 < P < 2.8$ atm) [45].

Overall, **Table 3** includes the experimental positions of 39 transitions ranging from the $S(0)$ pure rotational line near 354 cm^{-1} up to the $S(1)$ transition of the (5-0) band near 18908 cm^{-1} . Intensity measurements were performed for 34 transitions. In **Fig. 6**, laboratory observations including our CRDS measurements of five (2-0) transitions measurements are presented superimposed to the calculated spectrum. From this figure, it appears that (i) the (2-0) $O(4)$, $O(5)$ and $Q(5)$ transitions presently measured by CRDS are the weakest H_2 lines detected so far, (ii) the smallest measured intensity is about 10^{-30} cm/molecule while four transitions - $O(2)$ and $O(3)$ of (1-0) and $S(2)$ and $S(3)$ of (2-0)- with intensities on the order of 10^{-27} cm/molecule have not yet been measured, (iii) O branch transitions were measured only for the (2-0) band.

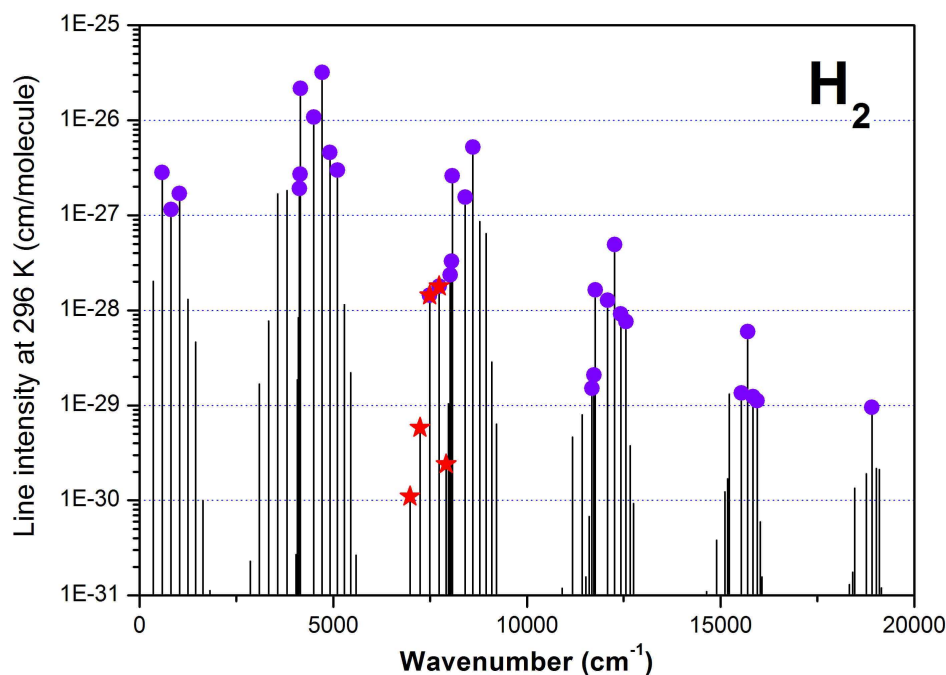


Fig.6

6. COMPARISON THEORY-EXPERIMENT

Line positions

We present in **Fig. 7**, the differences between the experimental values of the line positions and their calculated values. Excluding the (3-0) values reported in Ref. [45] with large error bar ($\pm 0.03 \text{ cm}^{-1}$), the comparison applies to 55 measurements. As indicated in **Table 3**, some line positions measured only at high pressure could not be corrected from the pressure shifts. As expected, their deviations are all negative (see **Fig. 7**). The error bars on the line positions as given in the original works are reproduced in **Table 3**. We present in **Fig. 8**, the (meas.-calc.) differences for the 31 positions corrected of the pressure shift and reported with an error bar. As an indication of the agreement with the theoretical values of the position of these 31 lines, we have included in **Table 3** the value of the “agreement factor”, A_p , defined as the ratio of the (meas.-calc.) deviations by the error bars. The agreement between theoretical and experimental values within their claimed error bars corresponds to absolute values of A_p smaller than 1. About half of the reported values agree with the theoretical values. Even if no global tendency is evidenced, a number of significant disagreements are noted:

(i) the very accurate positions of the pure rotational lines obtained by Jennings and Brault [25] show deviations which are ten times larger than both their experimental and theoretical uncertainties (see **Table 4**). For instance, the $S(3)$ position at 1034 cm^{-1} is given with a $3\times 10^{-5}\text{ cm}^{-1}$ error bar while it deviates by more than $5\times 10^{-4}\text{ cm}^{-1}$, the differences increasing up to $2\times 10^{-3}\text{ cm}^{-1}$ for $S(5)$. In principle, the shift of the line centers induced by collision is expected to be very weak for rotational transitions (Reid and McKellar reported an upper limit of $3\times 10^{-4}\text{ cm}^{-1}/\text{amagat}$ for the $S(3)$ line [38]). Nevertheless, a possible explanation for the observed deviations is that their experimental values were obtained at 1-2.2 atm and may be affected by a small pressure shift increasing with the rotational quantum number; which is consistent with the negative sign of the deviations. In order to examine this situation, we compare in **Table 4** the experimental [25] and theoretical values of the line positions to the accurate values at zero density obtained by Michaut et al. from stimulated Raman spectra [54]. A better agreement with theory is noted for values reported by Michaut et al.. Nevertheless, we note that the two experimental determinations of the $S(3)$ position fall in coincidence but show a deviation with theory which is five times larger than both the experimental and theoretical error bars. We have no explanation for this disagreement.

(ii) the position values given by Bragg et al. [17] are overestimated by about 1×10^{-3} and $4\times 10^{-3}\text{ cm}^{-1}$ for most of the (1-0) and (2-0) transitions, respectively. These differences are several times larger than the claimed uncertainties. In order to understand the origin of the discrepancy, we have considered the accurate transition frequencies at zero density measured by Rahn and Rosasco for the Raman (1-0) $Q(J)$ transitions ($J= 0-5$) [55] (**Table 4**). If we except the $Q(1)$ position which was adjusted according to Bragg et al. [17], the Raman values show a very good agreement with the theoretical predictions (deviations of $2\times 10^{-4}\text{ cm}^{-1}$ for $Q(2)$, $Q(3)$ and $Q(4)$) indicating a probable calibration problem of the spectra of Bragg et al.. The same reason is probably responsible for the $4\times 10^{-3}\text{ cm}^{-1}$ shift of the (2-0) transitions as Bragg et al. used the calibration in the (1-0) region to calibrate the (2-0) region [17]. This is confirmed by our CRDS measurements of (2-0) $O(2)$ and $O(3)$ transitions which coincide with the theoretical positions within our experimental uncertainty better than $1\times 10^{-3}\text{ cm}^{-1}$,

(iii) at higher energy, only the low pressure values of the (4-0) $S(0)$ and $S(1)$ positions are available. The $S(1)$ position reported with a $1\times 10^{-3}\text{ cm}^{-1}$ uncertainty by both Ferguson et al. [46] and Brault and Smith [47] differs by $6.6\times 10^{-3}\text{ cm}^{-1}$, the value of Ferguson et al. being in perfect agreement with the theoretical value.

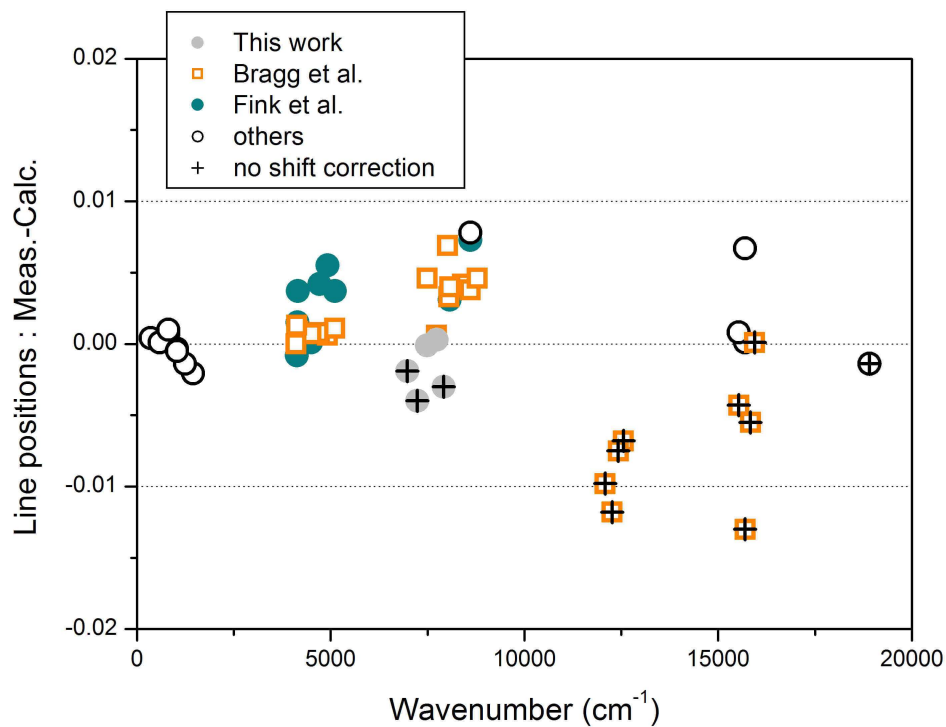


Fig. 7

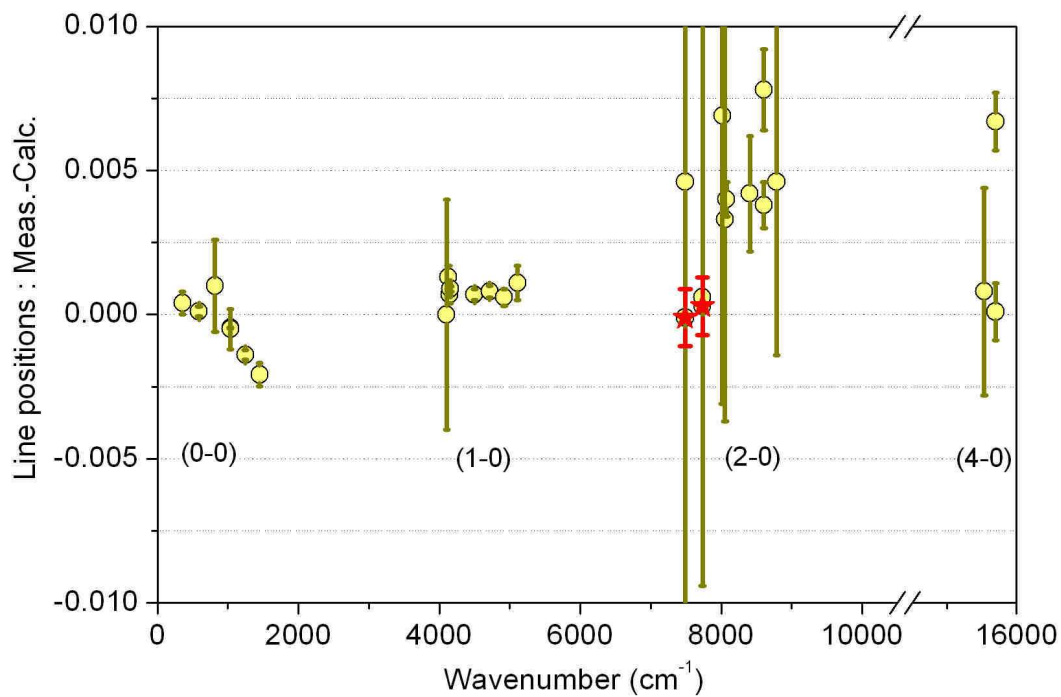


Fig. 8

Line intensities

The absolute intensity values are included in **Table 3** together with their claimed uncertainties and the relative difference, (meas./calc.-1), between the experimental and theoretical intensity values. The corresponding plot of the deviations is presented in **Fig. 9**. For an easier discussion of the quality of the agreement with theory, we provide for each line the value of the “agreement factor”, A_i , defined as the ratio of the (meas.-calc.) difference by the error bar on the experimental value (see **Table 3**). Over 47 measurements, the absolute values of A_i fall in the 0-1 and 1-2 intervals for 20 and 12 values, respectively. A careful examination of the A_i values shows a few cases where experimental values don't coincide within their claimed uncertainties. As an example we present in **Fig. 10**, the plot of the intensity ratios versus the line intensities for the (2-0) transitions. A very good agreement (within 1%) is noted between the theoretical value and the three available experimental values of the $S(1)$ intensity [17,40,42]. The situation is less satisfactory for the $Q(1)$ line for which the three experimental values [17,37,40,44] differ from the theoretical value by +11.7, -2.6 and +4.8 %; this last value being much larger than its claimed uncertainty of 0.06 %. We note the excellent coincidences (0.1 and 0.6 %) for the CRDS intensities of the $O(2)$ and $O(3)$ transitions while for the much weaker $O(4)$, $O(5)$ and $Q(5)$ lines the deviations are limited to 8% at most.

Contrary to the (2-0) and (1-0) transitions for which experimental and calculated intensity values show an overall satisfactory agreement, the experimental values of the higher overtone transitions appear to be systematically underestimated (lower panel of **Fig. 9**). Even if the relative uncertainties are increased as a result of the weakness of these transitions, the tendency seems significant. This disagreement was underlined by Robie and Hodges [44] who reported (3-0) intensity values with an uncertainty of about 2% while the underestimations from the theoretical values reach values around 30% for the Q lines [45].

Practically none of the experimental papers reporting H_2 intensity values with error bars provides detailed information on the fraction of the uncertainty due to experimental factors or to the line profile treatment. Indeed, besides the usual parameters contributing to the uncertainty on the absolute line strengths (sample pressure, sample purity, temperature, pathlength, superposition with impurity lines), the retrieved intensities may be affected by particular pressure effects affecting the line shape. Collisional effects show up in several manners for H_2 transitions: (i) the H_2 quadrupole lines display a marked Dicke narrowing as illustrated above by the analysis of the CRDS spectrum of the (2-0) lines (ii) electric dipole moments induced by collision lead to the appearance of collision induced absorption (CIA)

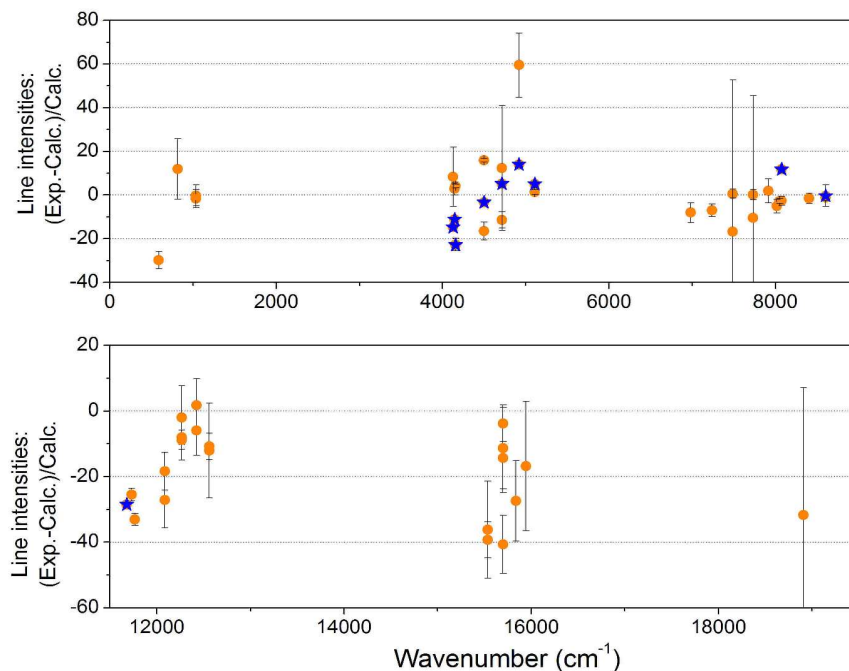
bands which are broad features ($> 100 \text{ cm}^{-1}$) centered at the frequency (or sum of frequencies) of the quadrupole transitions. The H_2 CIA band intensities are quadratic function of the molecular density. They have been extensively studied both theoretically and experimentally in a large range of pressure and temperature values [63-79], (iii) H_2 line profile may exhibit an unusual contribution resulting from intercollisional interference between the pressure-induced transition moments. It leads to the depletion of the CIA around the quadrupole frequency i.e. that the narrow quadrupole line is observed superimposed on a local minimum (a “dip”) of the CIA, the CIA contributing to a flat baseline of the spectrum.

Such dips were observed and studied in details for the (1-0) transitions recorded by Bragg et al. [17,75] with pressure values up to 2.8 atm. The intensity values reported by Bragg et al. (**Table 3**) were obtained by fitting independently the quadrupole line profile with a Galatry function and the “dip” with a Voigt function with a larger width (HWHM on the order of $0.05 \text{ cm}^{-1}/\text{amagat}$). A more sophisticated approach was developed by Kelley and Bragg to account for the same experimental data [75]: the observed asymmetry of the line shape was attributed to collisional phase shift and could be reproduced satisfactorily. The observation of absorption dips have also been observed in the CIA bands of H_2 in pure medium [78] or in H_2 -rare gas mixture [76,77], recorded at high pressure and low temperature spectra. The absorption dips are prominent in Q lines but they have also been detected in S transitions of the fundamental band [76,77]. Note that the (1-0) $Q(0)$ dip was observed while the corresponding quadrupole line is forbidden by the selection rules [75,77]. In the rotational region, Bachet reported the observation of a dip due to intercollisional interference effect at the frequency of the $S(1)$ line [79].

In the overtone region, Bragg et al. did not observe collisional dips in their high resolution spectra recorded at 2.8 atm. This observation is confirmed by all the measurements listed in **Table 3** obtained at moderate densities, in particular the high resolution laser studies of Refs. [42,46]. In spite of a very high signal to noise, our CRDS measurements of the first overtone transitions did not reveal significant deviation from the Galatry profile. This is consistent to the fact that, relative to the quadrupole lines, the CIA bands are weaker for higher overtones. To the best of our knowledge, the only experimental evidence of dips in the overtone region was obtained at very high pressure: Brodbeck et al. reported a sharp absorption feature around the $Q(1)$ frequency the (3-0) CIA band recorded with gas densities ranging from 100 to 800 amagats [68].

The possible relation between the collisional interference dips and the discrepancy between theoretical and measured intensities of the overtone transitions ($V > 2$) has been

considered by Robie [80]. From pulsed CRDS spectra of the (3-0) band, Robie and Hodges retrieved line strengths values which are systematically below the theoretical values, the discrepancy varying between 8 and 30 % [45]. The fact that the deviations are more pronounced for the *S* lines (about 10 %) than for the *Q*(1)–*Q*(3) lines (up to 30 %), may indicate that collisional dips alter the retrieved intensity values. In Ref. [80], Robie discussed quantitatively these experimental results and suggested that the discrepancy comes from the existence of a narrow “dip” in the quadrupole line profile which could not be observed due to the lack of resolution of the pulsed CRDS spectra of Ref. [45] (0.02 cm^{-1}). His calculations assume a 100 % depletion of the CIA at the maximum of the dip profile and a dip HWHM of $0.05 \text{ cm}^{-1}/\text{amagat}$ as determined by Bragg for the fundamental band [17,75]. Robie estimated to 5% the error on the (3-0) *S*(1) line strength due to the neglect of the narrow underlying dip, in good agreement with the 8% measured deviation [80]. However, his calculations are independent of the rovibrational transitions and cannot account for discrepancies larger than 5 %. For instance, his simple model cannot account for the discrepancies on the order of 30 % observed for the *Q* lines (in particular *Q*(1) for which a dip has been observed in the CIA [76]).

**Fig. 9**

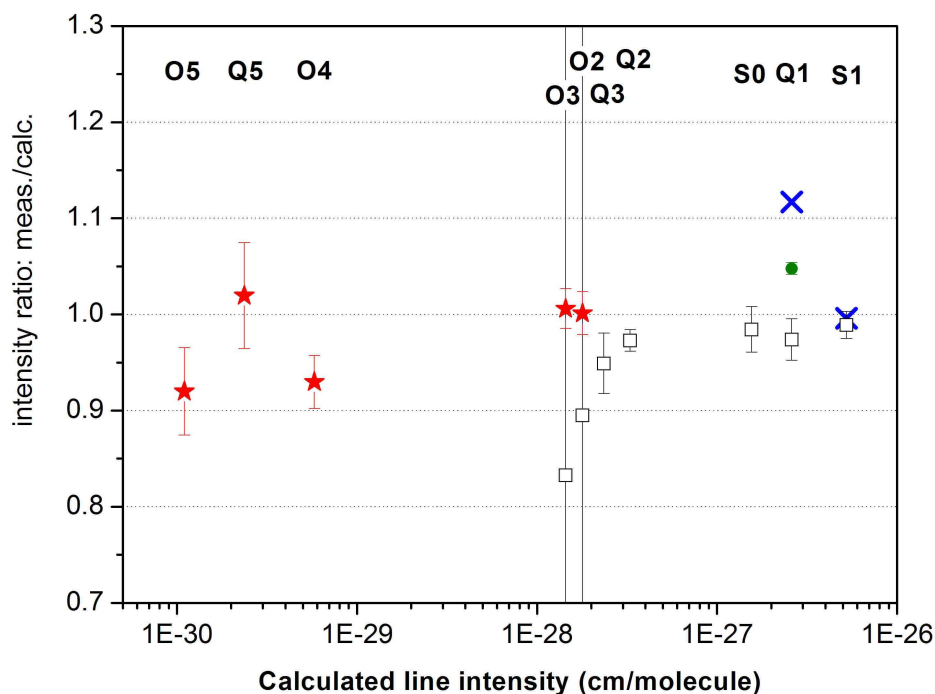


Fig.10

7. CONCLUSION

On the basis of the most advanced theoretical calculations [36], we have constructed a highly accurate and complete theoretical line list for pure H₂ for the whole 0-35000 cm⁻¹ range. To the best of our knowledge, no similar data set was previously released. Following the conventions adopted for the HTRAN database, the line strengths are given in cm/molecule at the reference temperature $T=296$ K. The list attached as Supplementary material includes the whole set of 175 quadrupole electric transitions which have intensity larger than 1×10^{-34} cm/molecule for pure H₂ at 296 K and the accurate lower state energies necessary to extrapolate the line intensities at different temperature. Note that the H₂ partition function was recently obtained in Ref. [81] from the direct summation of the energy levels calculated in Ref. [34]. The TIPS2011 program on the HITRAN website [21] allows calculating the partition functions at each temperature below 3000 K.

Theoretical position and intensity values have been systematically compared to laboratory measurements. The comparison was based on an exhaustive review of the literature data from pure rotational transitions up to (5-0) *S*(1) near 18907 cm⁻¹, which were gathered with new highly accurate measurements of five lines of the (2-0) band - *O*(2)-*O*(5) and *Q*(5) - recorded by high sensitivity CW-Cavity Ring Down Spectroscopy. Overall, experimental

information concerns 39 of the 175 transitions of the theoretical line list. The (2-0) $O(5)$ transition measured in this work is the weakest H_2 absorption line detected so far (intensity of about 1.1×10^{-30} cm/molecule). With the sensitivity achieved by cavity enhanced techniques, a number of new lines should be easily measured, in particular the six lines with intensity larger than 1.0×10^{-28} cm/molecule which have not been detected yet (see **Fig. 6**).

We have carefully examined and discussed the occurrences of discrepancies between experiment and theory, in particular for intensities. A general agreement has been evidenced for line positions. After correction of the pressure shift, many experimental values agree with theory within their quoted error bars (0.001 cm^{-1} for (2-0) transitions). Consequently, the H_2 calculated transition frequencies can be used as reference frequencies with an absolute uncertainty on the order of $1 \times 10^{-3} \text{ cm}^{-1}$ in the near infrared up to $5 \times 10^{-3} \text{ cm}^{-1}$ at 35000 cm^{-1} . As a side product of these calculations, we provide in **Table 5** the usual vibrational term and rotational constants for the $V=0-13$ vibrational states, obtained from the fit of the $J=0-7$ calculated rotational levels [36].

The uncertainty of the experimental intensity values is generally much larger than the claimed uncertainty of the theoretical values (0.1 %). Even if some conflicting results have been reported for the intensity of the (0-0), (1-0) and (2-0) transitions, the overall agreement is reasonable for these bands. Nevertheless, the twelve intensity measurements available for overtone transitions with $V>2$ are significantly below the theoretical values. The origin of this discrepancy remains open. We cannot rule out that particular collisional effects affecting the H_2 line shape have originated biases in the intensity retrievals. New recordings are then suitable to confirm the values of the overtone intensities which were all reported in the 80's and 90's. The improved performances provided nowadays by cavity enhanced absorption techniques should allow performing these recordings at low pressure (a few Torr) which will limit the impact of collisional effects.

Our similar CRDS study of the electric quadrupole and dipole transitions of the first overtone band of HD [62] has also illustrated the very high accuracy of the most advanced theoretical calculations of the electric dipole and electric quadrupole transitions in HD.

These results confirm that hydrogen isotopologues are among the few cases in rovibrational spectroscopy for which first principles theory competes with the best to date experimental techniques. While the 0.1 % accuracy claimed for the calculated intensities is probably out of reach experimentally, frequency comb assisted frequency measurements should provide position values with a much better accuracy than the 10^{-3} cm^{-1} accuracy claimed by theory. Line centre frequencies which can now be retrieved with an uncertainty of

30 kHz (10^{-5} cm⁻¹) [82], provide crucial tests for the relativistic and quantum electrodynamics corrections included in the *ab initio* calculations. Note that a complementary test on the ground electronic rotational levels ($J= 6-16$) is currently in progress by two-photon Doppler free spectroscopy of hot H₂ with a non thermal population distribution [83].

Acknowledgements

Helpful suggestions from R. Mc Kellar (NRC-Ottawa) and I. Gordon (Harvard-Smithsonian Centre for Astrophysics) are warmly acknowledged. K.P. and J.K. acknowledge the support of the Polish Ministry of Science and Higher Education *via* Grants No. N N204 182840 and No. N N204 015338, correspondingly. Part of the computations has been performed within a computing grant from Poznań Supercomputing and Networking Center.

Figure Captions**Fig. 1.**

Comparison of the profile of the $O(2)$ transition at 50 Torr and 700 Torr. For the clarity of the figure, the absorption coefficients have been divided by the pressure values in Torr. Note the pressure shift on the order of $-3 \times 10^{-3} \text{ cm}^{-1}$.

Fig. 2.

Line profile simulation of the (2-0) $O(2)$ transition at 700 Torr.

Upper panel: Experimental spectrum (dots), simulation using a Galatry profile (red line).

Lower panels: Residuals between the experimental and simulated spectra for the Voigt, Rautian and Galatry profiles. Note the different scale used for the residuals.

Fig. 3.

Line profile simulation of the $O(3)$ and $Q(5)$ transitions at 7.00 and 700.0 Torr, respectively.

Upper panels: Experimental spectra

Lower panels: Residuals between the experimental spectra and the simulation using a Galatry profile. In the case of the $Q(5)$ line, the *rms* of the residuals is close to the noise equivalent absorption ($\alpha_{\text{min}} \approx 5 \times 10^{-11} \text{ cm}^{-1}$). The presence of a line due to oxygen (O_2) was taken into account in the fit of the $Q(5)$ transition.

Fig. 4.

Line intensity and pressure shift retrieval for the (2-0) $O(2)$ and $O(3)$ transitions.

Left panel: Variation of the integrated absorption coefficient at 294 K obtained with a Galatry profile fit versus the pressure. The straight lines correspond to the best linear fit (regression coefficient of 0.99998 for both).

Right panel: Variation of the line centre versus the pressure values. The $O(2)$ and $O(3)$ positions correspond to the right and left scales, respectively.

Fig. 5.

Overview of the calculated spectrum of H_2 between 0 and 35000 cm^{-1} .

Fig. 6.

Overview of the laboratory measurements of H_2 transitions available in the literature (full dots) and presently reported by CW-CRDS (stars).

Fig. 7.

Differences between the measured and calculated line positions of the H_2 transitions measured by absorption spectroscopy (see **Table 3**). The crosses (+) indicate the measurements which were reported without pressure shift correction.

Fig. 8.

Differences between the zero density line positions and the calculated line positions for the H_2 transitions measured by absorption spectroscopy (see **Table 3**). This plot is limited to the transitions corrected from pressure shift. The $O(2)$ and $O(3)$ measurements by CRDS are marked with star.

Fig. 9.

Relative differences, $(\text{Exp.}-\text{Calc.})/\text{Calc.}$, between the measured and calculated line strengths of H_2 (see Table 3). The stars correspond to measurements reported without error bars. Note that all but one of the values of the lower panel are negative.

Fig. 10.

Intensity ratio, $\text{Meas.}/\text{Calc.}$, for the (2-0) transitions versus the calculated intensity values. Different symbols are used for each experimental source: This work: stars, Bragg et al. [17]: open squares (\square), Gupta et al. [42]: full dot (\bullet), Fink et al. [40]: crosses (\times).

References

1. G. Herzberg, *Nature*, 1949, **163**, 170-170.
2. W. H. Smith, C. P. Conner, J. Simon, W. V. Schempp and W. Macy, *Icarus*, 1989, **81**, 429-440.
3. K. H. Baines, M. E. Mickelson, L. E. Larson, D. W. Ferguson, *Icarus*, 1995, **114**, 328-340.
4. D. Goorvitch, C. Chackerian, Jr., *Icarus*, 1977, **32**, 348-361.
5. W. H. Smith, C. P. Conner, K. H. Baines, *Icarus*, 1990, **85**, 58-64.
6. W. H. Smith, K. H. Baines, *Icarus*, 1990, **85**, 109-119.
7. L. Trafton, *Icarus*, 1987, **70**, 13-30.
8. R. W. McKellar, *Icarus*, 1974, **22**, 212-219.
9. G. Karl and J. D. Poll, *J. Chem. Phys.* 1967, **46**, 2944-50.
10. L. Wolniewicz, I. Simbotin, and A. Dalgarno, *Astrophys. J., Suppl. Ser.* 1998, **115**, 293-313.
11. L. Wolniewicz, *Can. J. Phys.* 1975, **53**, 1207-14.
12. L. Wolniewicz, *Can. J. Phys.* 1976, **54**, 672-79.
13. J.L. Hunt, J.D. Poll, L. Wolniewicz, *Can. J. Phys.* 1984, **62**, 1719-23.
14. L. Wolniewicz, *J. Chem. Phys.* 1995, **103**, 1792-99.
15. C. Schwartz and R.J. Le Roy, *J. Mol. Spectrosc.* 1987, **121**, 420-39.
16. K. Pachucki, *Phys. Rev. A*, 2010, **82**, 032509.
17. S. L. Bragg, J. W. Brault, W. H. Smith, *Astrophys. J.*, 1982, **263**, 999-1004.
18. J. Morville, D. Romanini, A.A. Kachanov, M. Chenevier, *Appl. Phys.* 2004, **D78**, 465-76.
19. P. Macko, D. Romanini, S.N. Mikhailenko, O.V. Naumenko, S. Kassi, A. Jenouvrier, V.I.G. Tyuterev and A. Campargue. *J. Mol. Spectrosc.* 2004, **227**, 90-108.
20. B.V. Perevalov, S. Kassi, D. Romanini, V.I. Perevalov, S.A. Tashkun, A. Campargue, *J. Mol. Spectrosc.* 2006, **238**, 241-55.
21. L.S. Rothman, I.E. Gordon, A. Barbe, D. Chris Benner, P.F. Bernath, M. Birk, V. Boudon, L.R. Brown, A. Campargue, J.-P. Champion, K. Chance, L.H. Coudert, V. Dana, V.M. Devi, S. Fally, J.-M. Flaud, R.R. Gamache, A. Goldman, D. Jacquemart, I. Kleiner, N. Lacome, W. J. Lafferty, J.-Y. Mandin, S.T. Massie, S.N. Mikhailenko, C.E. Miller, N. Moazzen-Ahmadi, O.V. Naumenko, A.V. Nikitin, J. Orphal, V.I. Perevalov, A. Perrin, A. Predoi-Cross, C.P. Rinsland, M. Rotger, M. Šimečková, M.A.H. Smith, K. Sung, S.A. Tashkun, J. Tennyson, R.A. Toth, A.C. Vandaele and J. Vander Auwera, *J. Quant. Spectrosc. Radiat. Transfer.*, 2009, **110**, 533-572.
22. R. L. Farrow, R. E. Palmer, *Opt. Lett.*, 1987, **12**, 984-986.
23. H. Tran, J.-M. Hartmann, F. Chaussard and M. Gupta, *J. Chem. Phys.* 2009, **131**, 154303-1-9.
24. J. D. Kelley, S. L. Bragg, *Phys. Rev. A*, 1986, **34**, 3003-3014.
25. D. E. Jennings, J. W. Brault, *J. Mol. Spectrosc.*, 1983, **102**, 265-272.
26. K. Pachucki, *Phys. Rev. A*, 2005, **71**, 012503.
27. K. Pachucki, *Phys. Rev. A*, 2006, **74**, 022512.
28. K. Pachucki and J. Komasa, *J. Chem. Phys.*, 2009, **130**, 164113
29. W. Cencek (2003), *private communication*.
30. J. Sims and S. Hagstrom, *J. Chem. Phys.* 2006, **124**, 094101.
31. J. Rychlewski and J. Komasa, "Explicitly correlated functions in variational calculations.", Explicitly Correlated Wave Functions in Chemistry and Physics (edited by J.Rychlewski) Kluwer Academic Publishers, Dordrecht, 2003, p. 91-147
32. K. Pachucki and J. Komasa, *Phys. Rev. A*, 2011, **83**, 032501.
33. K. Pachucki and J. Komasa, *J. Chem. Phys.*, 2008, **129**, 034102.
34. K. Piszczatowski, G. Łach, M. Przybytek, J. Komasa, K. Pachucki and B. Jeziorski, *J. Chem. Theory Comput.*, 2009, **5**, 3039-3048.
35. K. Pachucki and J. Komasa, *J. Chem. Phys.*, 2009, **130**, 164113
36. J. Komasa, K. Piszczatowski, G. Łach, M. Przybytek, B. Jeziorski, and K. Pachucki, *submitted to JCTC*.
37. G. Chackerian, Jr and L. P. Giver Applied Optics 1975, **14**, 1993-1996.
38. J. Reid, A. R. W. McKellar, *Phys. Rev. A*, 1978, **18**, 224-228.
39. D. E. Jennings, J. W. Brault, *Astrophys. J.*, 1982, **256**, L29-L31.
40. U. Fink, T. A. Wiggins, D. H. Rank, *J. Mol. Spectrosc.*, 1965, **18**, 384-395.
41. J. S. Margolis, *J. Mol. Spectrosc.*, 1973, **48**, 409-410.
42. M. Gupta, T. Owano, D. S. Baer, A. O'Keefe, *Chem. Phys. Lett.*, 2006, **418**, 11-14.
43. D. C. Reuter, J. M. Sirota, *Astrophys. J.*, 1994, **428**, L77-L79.
44. C. Chackerian, Jr., L. P. Giver, *J. Mol. Spectrosc.*, 1975, **58**, 339-343.
45. D. C. Robie, J. T. Hodges, *J. Chem. Phys.*, 2006, **124**, 024307(1-5).
46. D. W. Ferguson, K. N. Rao, M. E. Mickelson, L. E. Larson, *J. Mol. Spectrosc.*, 1993, **160**, 315-325.
47. J. W. Brault, W. H. Smith, *Astrophys. J.*, 1980, **235**, L177-L178.
48. J. T. Trauger, M. E. Mickelson, L. E. Larson, *Astrophys. J.*, 1978, **225**, L157-L160.

49. B. P. Stoicheff, *Can. J. Phys.*, 1957, **35**, 730-741.
50. D. K. Veirs, G. M. Rosenblatt, *J. Mol. Spectrosc.*, 1987, **121**, 401-419.
51. D. E. Jennings, A. Weber, J. W. Brault, *J. Mol. Spectrosc.*, 1987, **126**, 19-28.
52. J. V. Foltz, D. H. Rank, and T. A. Wiggins, *J. Mol. Spectrosc.* 1966, **21**, 203-216.
53. G. J. Germann, and J. J. Valentini, *J. Phys. Chem.* 1987, **92**, 3792-3795.
54. X. Michaut, R. Saint-Loup, H. Berger, M. L. Dubernet, P. Joubert, and J. Bonamy, *J Chem Phys*, 1998, **109**, 951-62.
55. L. A. Rahn, G. J. Rosasco, *Phys. Rev. A*, 1990, **41**, 3698-3706.
56. P. J. Brannon, C. H. Church, C. W. Peters, *J. Mol. Spectrosc.*, 1968, **27**, 44-54.
57. R.F. Knacke and E. T Young, *Astrophys. J.*, 1981, **249**, L65-L69.
58. G. Herzberg, L. L. Howe, *Can. J. Phys.*, 1959, **37**, 636-659.
59. I. Dabrowski, *Can. J. Phys.*, 1984, **62**, 1639-1664.
60. D. H. Rank, U. Fink, T. A. Wiggins, *Astrophys. J.*, 1966, **143**, 980-988. useless
61. D. W. Steyert, J. M. Sirota, M. E. Mickelson, D. C. Reuter, *Rev. Sci. Instrum.*, 2001, **72**, 4337-4343.
62. S. Kassi and A. Campargue, *J. Mol. Spectrosc.* 2011, **267**, 36-42.
63. R. W. McKellar, *Can. J. Phys.*, 1988, **66**, 155-158.
64. R. D. G. Prasad, P. G. Gillard, S. P. Reddy, *J. Chem. Phys.*, 1997, **107**, 4906-4910.
65. W. Meyer, A. Borysow, L. Frommhold, *Phys. Rev. A*, 1989, **40**, 6931-6949.
66. W. Meyer, A. Borysow, L. Frommhold, *Phys. Rev. A*, 1993, **47**, 4065-4077.
67. Y. Fu, C. Zheng, A. Borysow, *J. Quant. Spectrosc. Radiat. Transfer*, 2000, **67**, 303-321.
68. C. Brodbeck, J.-P. Bouanich, Nguyen-van-Thanh, Y. Fu, A. Borysow, *J. Chem. Phys.*, 1999, **110**, 4750-4756.
69. A. Borysow, J. Borysow, Y. Fu, *Icarus*, 2000, **145**, 601-608.
70. A. Borysow, U. G. Jorgensen, Y. Fu, *J. Quant. Spectrosc. Radiat. Transfer*, 2001, **68**, 235-255.
71. M. Abel, L. Frommhold, M. Gustafsson, *J. Chem. Phys.*, 2009, **131**, 181102(1-3).
72. M. Abu-Kharma, C. Stamp, G. Varghese, S. P. Reddy, *J. Quant. Spectrosc. Radiat. Transfer*, 2006, **97**, 332-343.
73. P. M. Silvaggio, D. Goorvitch, R. W. Boese, *J. Quant. Spectrosc. Radiat. Transfer*, 1981, **26**, 103-106.
74. M. Abel, L. Frommhold, X. Li, K. L. C. Hunt, *J. Phys. Chem. A*, 2011, **115**, 6805-6812.
75. J. D. Kelley, S. L. Bragg, *Phys. Rev. A*, 1984, **29**, 1168-1173.
76. D. Poll, J. L. Hunt, J. W. Mactaggart, *Can. J. Phys.*, 1975, **53**, 954-961.
77. A. R. W. McKellar, J. W. Mactaggart, H. L. Welsh, *Can. J. Phys.*, 1975, **53**, 2060-2067.
78. S. P. Reddy, G. Varghese, R. D. G. Prasad, *Phys. Rev. A*, 1977, **15**, 975-984.
79. G. Bachet, *J. Phys. Lett.*, 1983, **44**, 183-187.
80. D. C. Robie, *Chem. Phys. Lett.*, 2006, **428**, 39-41.
81. A.L. Laraia, J. Lamouroux, R.R. Gamache, I.E. Gordon, L.S. Rothman, *Icarus*, in press (2011)
doi:10.1016/j.icarus.2011.06.004
82. D. Gatti, A. Gambetta, A. Castrillo, G. Galzerano, P. Laporta, L. Gianfrani, M. Marangoni, *Opt. Exp.*, 2011, **19**, 17520-17527.
83. E. J. Salumbides, G. D. Dickenson, T. I. Ivanov, W. Ubachs, *Phys. Rev. Lett.* submitted.

Table 1. Centres and intensities for the transitions of the (2-0) H₂ band measured by CRDS between 6900 and 7920 cm⁻¹.

Transition	Position (cm ⁻¹)			Intensity (10 ⁻³⁰ cm/molecule)			Intensity ratio Meas./Calc.
	Measured		Calculated	Measured		Calculated	
	0 Torr	700 Torr		294 K	296 K		
O5		6982.5105	6982.5124	0.964	1.015	1.0980	0.924
O4		7237.5594	7237.5634	5.222	5.395	5.7974	0.931
O3	7488.2753	7488.2721	7488.2754	142.8	145.3	144.1	1.008
	7488.28(2) ^a				122.8		0.852
O2	7732.6297	7732.6263	7732.6294	178.1	179.0	178.8	1.001
	7732.63(1) ^a				163.8		0.916
Q5		7914.0040	7914.0070	2.292	2.413	2.365	1.020

^a Ref. [17].

Table 2.

Calculated values of the position, intensity, lower state energy and transition moment for the (2-0) transition of H₂. This Table is a sample of the whole calculated line list, provided as Supplementary Material, for pure H₂ up to 35000 cm⁻¹ (intensity cut off of 1×10⁻³⁴ cm/molecule).

Band	Transition	Position (cm ⁻¹)	Intensity (cm/molecule)	Lower state energy (cm ⁻¹)	Transition moment <V' <i>J'</i> Q(R) V'' <i>J''</i> > (a.u.) ^a
(2-0)	O7	6466.7267 (16)	7.978E-34	3187.4705	7.488007E-3
	O6	6725.0006 (16)	1.292E-32	2414.8970	8.191646E-3
	O5	6982.5124 (17)	1.099E-30	1740.1896	8.863463E-3
	O4	7237.5634 (17)	5.802E-30	1168.7975	9.491750E-3
	O3	7488.2754 (17)	1.443E-28	705.5189	1.006544E-2
	O2	7732.6295 (17)	1.789E-28	354.3732	1.057453E-2
	Q7	7768.1472 (17)	2.870E-33	3187.4705	1.218106E-2
	Q6	7846.2315 (17)	3.520E-32	2414.8970	1.193206E-2
	Q5	7914.0076 (17)	2.367E-30	1740.1896	1.171878E-2
	Q4	7971.1001 (17)	1.042E-29	1168.7975	1.154104E-2
	Q3	8017.1831 (17)	2.355E-28	705.5189	1.139881E-2
	Q2	8051.9877 (17)	3.291E-28	354.3732	1.129207E-2
	Q1	8075.3074 (17)	2.600E-27	118.4869	1.122088E-2
	S0	8406.3608 (18)	1.559E-27	0.0000	1.163673E-2
	S1	8604.2152 (18)	5.234E-27	118.4869	1.181921E-2
	S2	8785.5244 (18)	8.564E-28	354.3732	1.191243E-2
	S3	8948.6783 (18)	6.391E-28	705.5189	1.191695E-2
	S4	9092.3310 (18)	2.845E-29	1168.7975	1.183471E-2
	S5	9215.4281 (18)	6.366E-30	1740.1896	1.166867E-2
	S6	9317.2177 (18)	9.142E-32	2414.8970	1.142237E-2
S7	9397.2457 (18)	7.051E-33	3187.4705	1.109953E-2	

^a To convert from atomic unit (a.u.) to Debye multiply by 2.541 746 23 Debye/a.u.

Table 3.

Comparison of the calculated values of the position of the (0-0) and (1-0) transitions to experimental values obtained by Raman spectroscopy [54, 55] and absorption spectroscopy [17,25].

Band	Transition	Line position			A_p^b	Reference
		Calc. (cm ⁻¹)	Meas. (cm ⁻¹) ^a	Meas.-Calc. (10 ⁻³ cm ⁻¹)		
(0-0)	S(0)	354.37313(3)	354.37297(11)	-0.16	-1.4	Michaut et al.1998 [54] Jennings and Brault 1983 [25]
			354.37350(40)	0.37	0.9	
	S(1)	587.03202(4)	587.03200(13)	-0.02	-0.2	Michaut et al.1998 [54] Jennings and Brault 1983 [25]
			587.03211(17)	0.09	0.5	
	S(2)	814.42430(6)	814.42401(8)	-0.29	-3.6	Michaut et al.1998 [54] Jennings and Brault 1983 [25]
814.42473(8)			0.43	5.4		
S(3)	1034.67068(8)	1034.67026(6)	-0.42	-7.0	Michaut et al.1998 [54] Jennings and Brault 1983 [25]	
		1034.67024(3)	-0.44	-14.7		
S(4)	1246.09954(9)	1246.09923(19)	-0.31	-1.6	Michaut et al.1998 [54] Jennings and Brault 1983 [25]	
		1246.09811(17)	1.43	-8.4		
(1-0)	Q(5)	4073.7322(9)	4073.7326(14)	0.4	0.3	Rahn and Rosasco 1990 [55]
	Q(4)	4102.5820(9)	4102.5822(12)	0.2	0.2	Rahn and Rosasco 1990 [55] Bragg et al. 1982 [17]
			4102.582(4)	0.0	0.0	
	Q(3)	4125.8726(9)	4125.8728(14)	0.2	0.1	Rahn and Rosasco 1990 [55] Bragg et al. 1982 [17]
			4125.8739(4)	1.3	3.2	
	Q(2)	4143.4653(9)	4143.4651(14)	-0.2	-0.1	Rahn and Rosasco 1990 [55] Bragg et al. 1982 [17]
			4143.4660(3)	0.7	2.3	
Q(1)	4155.2538(9)	4155.2547(5)	0.9	1.8	Rahn and Rosasco 1990 [55] Bragg et al. 1982 [17]	
		4155.25469(8)	0.89	11.1		
Q(0)	4161.1662(9)	4161.1673(14)	1.1	0.8	Rahn and Rosasco 1990 [55]	

Band ($V'-V''$)	Transition	Line position					Line intensity				Reference
		Calc. (cm^{-1})	Meas. (cm^{-1}) ^a	Meas.-Calc. (10^{-3} cm^{-1})	A_p ^b	Shift coefficient ($10^{-3} \text{ cm}^{-1}/\text{amagat}$)	Calc. ($10^{-28} \text{ cm/molecule}$)	Meas. ($10^{-28} \text{ cm/molecule}$)	Relative difference (%)	A_i ^c	
(0-0)	S(0)	354.37313	354.37350(40)	0.4	0.9		2.024				Jennings and Brault 1983 [25]
	S(1)	587.03202	587.03211(17)	0.09	0.5		28.18	19.8(1.1)	-29.7	-7.6	Jennings and Brault 1983 [25] Reuter and Sirota 1994 [43]
	S(2)	814.42430	814.42473(8) 814.4250(5)	0.43 0.7	5.4 1.4		11.53	12.9(1.6)	11.9	0.9	Jennings and Brault 1983 [25] Jennings and Brault 1982 [39]
	S(3)	1034.67068	1034.67024(3) 1034.6702(7) 1034.67035(10)	-0.44 -0.5 -0.35	-14.7 -0.7 -3.5	<0.3	16.98	16.70(71) 16.94(81)	-1.6 -0.2	-0.4 -0.0	Jennings and Brault 1983 [25] Reid and McKellar 1978 [38] Jennings and Brault 1982 [39]
	S(4)	1246.09954	1246.09811(17)	-1.43	-8.4		1.3033				Jennings and Brault 1983 [25]
	S(5)	1447.28093	1447.27882(41)	-2.08	-5.1		0.4627				Jennings and Brault 1983 [25]
(1-0)	Q(4)	4102.5820	4102.582(4)	0	0	-1.7(1.9)	0.8345				Bragg et al. 1982 [17]
	Q(3)	4125.8726	4125.8718 4125.8739(4)	-0.8 1.3	3.2	-4.8(assumed) -2.2(2)	19.205	16.3724 20.8(2.6)	-14.7 8.3	0.6	Fink et al. 1965 [40] Bragg et al. 1982 [17]
	Q(2)	4143.4653	4143.4668y 4143.4660(3)	1.5 0.7	2.3	-2.4(assumed) -2.0(1)	27.217	24.1865 27.98(74)	-11.1 2.8	1.0	Fink et al. 1965 [40] Bragg et al. 1982 [17]
	Q(1)	4155.2538	4155.2575 4155.25469(8)	3.7 0.89	11.1	-2.40 -2.13(4)	217.000	167.445 225.9(1.8) 167.8(6.3)	-22.8 4.1 -22.7	4.9 -7.8	Fink et al. 1965 [40] Bragg et al. 1982 [17] Margolis 1973 [41]
	S(0)	4497.8384	4497.8385y 4497.8391(2)y	0.1 0.7	3.5	-1.67 -1.8(1)	107.817	104.188 125.03(86) 90.0(4.5)	-3.4 16.0 -16.5	20.0 -4.0	Fink et al. 1965 [40] Bragg et al. 1982 [17] Margolis 1973 [41]
	S(1)	4712.9046	4712.9088 4712.9054(2)	4.2 0.8	4.0	-2.40 -1.86(9)	318.508	334.89 358(91) 282(12)	5.1 12.4 -11.5	0.4 -3.0	Fink et al. 1965 [40] Bragg et al. 1982 [17] Margolis 1973 [41]
	S(2)	4917.0063	4917.0118 4917.0069(3)	5.5 0.6	2.0	-3.53 -1.4(1)	45.713	52.094 72.9(6.7)	14.0 59.5	4.1	Fink et al. 1965 [40] Bragg et al. 1982 [17]
	S(3)	5108.4029	5108.4066	3.7		-1.77	29.769	31.2564	5.0		Fink et al. 1965 [40]

			5108.4040(6)	1.1	1.8	-2.0(2)		30.18(30)	1.4	1.4	Bragg et al. 1982 [17]
(2-0)	O(5)	6982.5124	6982.5105	-1.9			0.01098	0.0101(5)	-8.0	-1.8	This work
	O(4)	7237.5634	7237.5594	-4			0.05797	0.0539(16)	-7.0	-2.5	This work
	O(3)	7488.2754	7488.2753 7488.28(2)	-0.1 4.6	0.1 0.2	-3.33(16) -5(10)	1.4414	1.45(3) 1.2(1.0)	0.6 -16.7	0.3 -0.2	This work Bragg et al. 1982 [17]
	O(2)	7732.6294	7732.6297 7732.63(1)	0.3 0.6	0.1 0.1	-3.62(14) -5(5)	1.7879	1.79(4) 1.6(1.0)	0.1 -10.5	0.1 -0.2	This work Bragg et al. 1982 [17]
	Q(5)	7914.0070	7914.0040	-3			0.02364	0.0241(13)	1.9	0.4	This work
	Q(3)	8017.1831	8017.19(1)	6.9	0.7	-4(4)	2.353	2.233(74)	-5.1	-1.6	Bragg et al. 1982 [17]
	Q(2)	8051.9877	8051.991(7)	3.3	0.5	-4(3)	3.289	3.200(37)	-2.7	-2.4	Bragg et al. 1982 [17]
	Q(1)	8075.3074	8075.3105 8075.3114(6)	3.1 4		-4.8(assumed) -4.8(2) -2.6	25.980	29.0238 25.30(56) 27.22	11.7 -2.6 4.8		Fink et al. 1965 [40] Bragg et al. 1982 [17] Gupta et al. 2006 [42]
	S(0)	8406.3608	8406.365(2)	4.2	2.1	-4.5(9)	15.574	15.33(37)	-1.6	-0.7	Bragg et al. 1982 [17]
	S(1)	8604.2151	8604.2224 8604.2189(8) 8604.2229(14)	7.3 3.8 7.8		-4.8(assumed) -4.3(3) -4.5(5)	52.301	52.094 51.73(74) 52.1(2.6)	-0.4 -1.1 -0.4		Fink et al. 1965 [40] Bragg et al. 1982 [17] Chackerian and Giver 1975 [34,44]
	S(2)	8785.5244	8785.529(6)	4.6	0.8	-4(3)	8.557				Bragg et al. 1982 [17]
(3-0)	Q(3)	11678.5629	11678.64(3)	77.1			0.1511	0.108	-28.5		Robie and Hodges 2006 [45]
	Q(2)	11730.3239	11730.36(3)n	36.1			0.2093	0.156(4)	-25.5	-13.3	Robie and Hodges 2006 [45]
	Q(1)	11765.0009	11765.01(3)	9.1			1.643	1.10(3)	-33.0	-18.1	Robie and Hodges 2006 [45]
	S(0)	12084.6970	12084.6872(23)	-9.8			1.276	1.042(74) 0.93(11)	-18.3 -27.1	-3.2 -3.1	Bragg et al. 1982 [13] Robie and Hodges 2006 [29]
	S(1)	12265.5949	12265.5831(7)	-11.8			4.936	4.50(30) 4.54(11) 4.84(48)	-8.8 -8.0 -1.9	-1.5 -3.6 -0.2	Bragg et al. 1982 [17] Robie and Hodges 2006 [45] Trauger et al. 1978 [48]

(4-0)	S(2)	12424.4421	12424.4346(37)	-7.5			0.9142	0.930(74) 0.86(7)	1.7 -5.9	0.2 -0.8	Bragg et al. 1982 [17] Robie and Hodges 2006 [45]
	S(3)	12559.7492	12559.7424(59)	-6.8			0.7621	0.67(11) 0.68(3)	-12.1 -10.8	-0.8 -2.7	Bragg et al. 1982 [17] Robie and Hodges [45]
	S(0)	15535.7433	15535.739(49) 15535.7441(36)	-4.3 0.8	0.2	-6.3(1.3)	0.1348	0.08186(74) 0.086(20)	-39.3 -36.2	-7.2 -2.4	Bragg et al. 1982 [17] Ferguson et al. 1993 [46]
	S(1)	15699.8010	15699.788(7) 15699.8077(10) 15699.8011(10)	-13 6.7 0.1	6.7 0.1	-7.0(1.5) -4.22(36)	0.5955	0.528(74) 0.573(33) 0.353(53) 0.510(63)	-11.3 -3.8 -40.7 -14.4	-0.9 -0.7 -4.6 -1.4	Bragg et al. 1982 [17] Brault and Smith 1980 [47] Trauger et al. 1978 [48] Ferguson et al. 1993 [46]
(5-0)	S(2)	15836.3295	15836.324(50)	-5.5			0.1227	0.089(15)	-27.5	-2.2	Bragg et al. 1982 [17]
	S(3)	15943.9499	15943.95(11)	0.1			0.1118	0.093(22)	-16.8	-0.9	Bragg et al. 1982 [17]
	S(1)	18907.5174	18907.5160(200)	-1.4			0.09521	0.065(37)	-31.7	-0.8	Ferguson et al. 1993 [46]

Table 4.

Review of the observations of H₂ absorption lines available in the literature and measured in this work and comparison of the positions and intensities to the corresponding calculated values.

Notes

^aIn absence of value in the pressure shift column, the value given for the measured position is not corrected from the pressure shift.

^b A_p : “agreement factor” for the positions: ratio of the difference of the measured and calculated line positions by the experimental error bar. The A_p values are given only for the lines corrected for the pressure shift. If $|A_p| < 1$, the measured and calculated line positions agree with each other.

^c A_i : “agreement factor” for the intensities: ratio of the difference of the measured and calculated line strength by the experimental error.

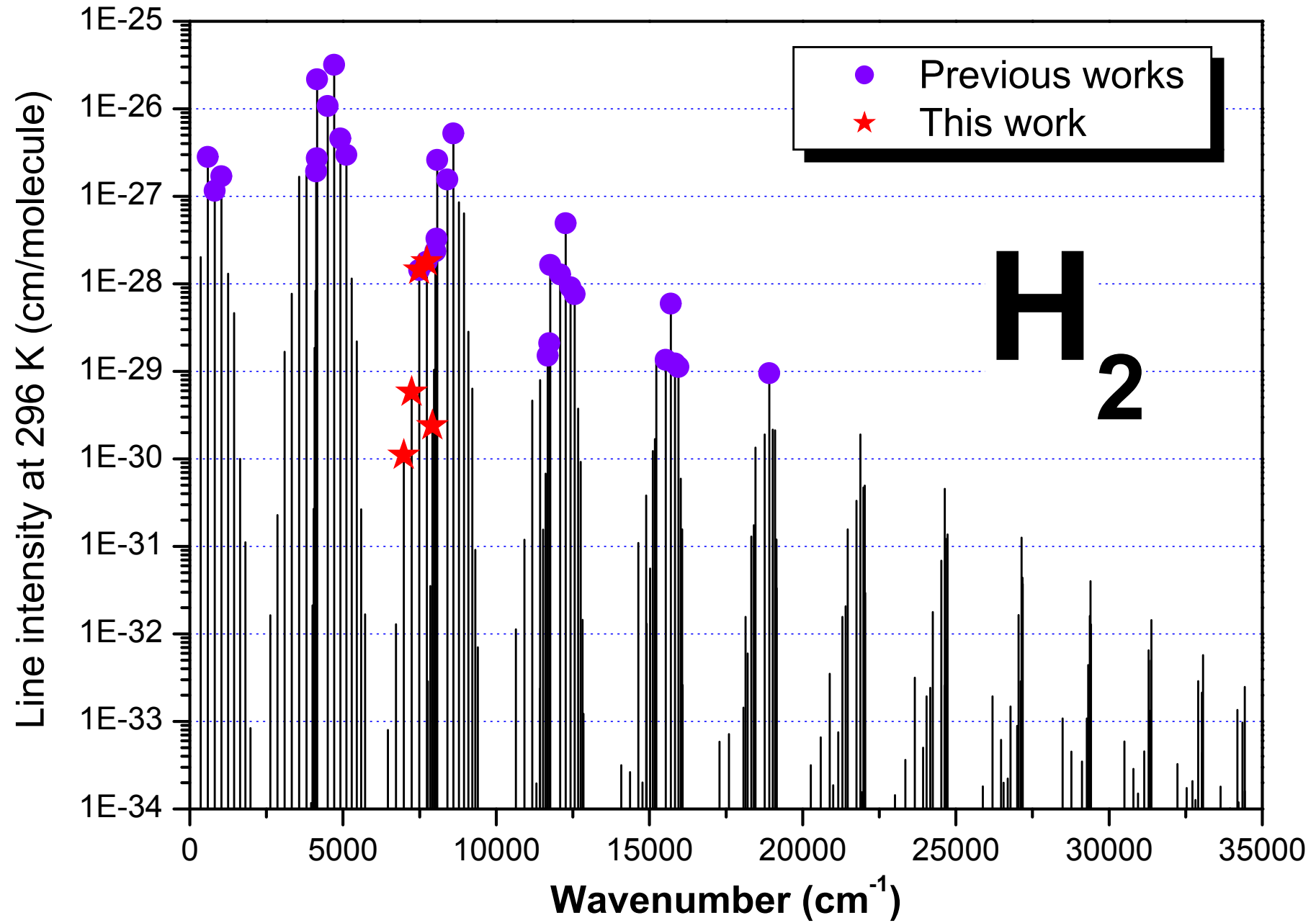
Table 5.

Rovibrational parameters of the $V=0-13$ vibrational levels of H_2 obtained from the fit of the $J=0-7$ energy levels calculated in Ref. [36].

V	$E_V(\text{cm}^{-1})$	$B_V(\text{cm}^{-1})$	$D_V(\text{cm}^{-1})$	$H_V(10^{-3}\text{cm}^{-1})$	$rms(10^{-3}\text{cm}^{-1})$
0	0.0(00)	59.33289(44)	-0.045498(24)	4.277(30)	3.4
1	4161.1693(32)	56.37318(66)	-0.043961(30)	4.168(36)	3.2
2	8087.0058(32)	53.47892(66)	-0.042523(30)	4.070(36)	3.2
3	11782.3940(32)	50.62885(65)	-0.041175(30)	3.963(36)	3.2
4	15250.3688(32)	47.79997(65)	-0.039927(30)	3.846(35)	3.2
5	18491.9328(32)	44.96596(66)	-0.038795(30)	3.717(36)	3.2
6	21505.7826(32)	42.09566(65)	-0.037808(30)	3.571(35)	3.1
7	24287.9184(31)	39.15105(64)	-0.037004(29)	3.399(35)	3.1
8	26831.0937(32)	36.08416(65)	-0.036451(30)	3.187(35)	3.1
9	29124.0436(32)	32.83233(66)	-0.036251(30)	2.902(36)	3.2
10	31150.3944(35)	29.31063(71)	-0.036582(33)	2.473(39)	3.4
11	32887.1026(43)	25.39856(89)	-0.037763(41)	1.711(48)	4.3
12	34302.1817(81)	20.9136(17)	-0.040392(76)	-0.065(90)	8.0
13	35351.357(48)	15.5356(98)	-0.04482(45)	-7.95(53)	47.6

Note

The usual expression of the vibration-rotational energy levels was used to fit the theoretical values: $F_v(J) = G_v + B_v J(J+1) - D_v J^2(J+1)^2 + H_v J^3(J+1)^3$ where G_v is the vibrational term value, B_v is the rotational constant, D_v and H_v are centrifugal distortion constants, J is the angular momentum quantum number. The expansion being limited to the first distortion terms, the obtained parameters are not expected to reproduce accurately high J energy levels.



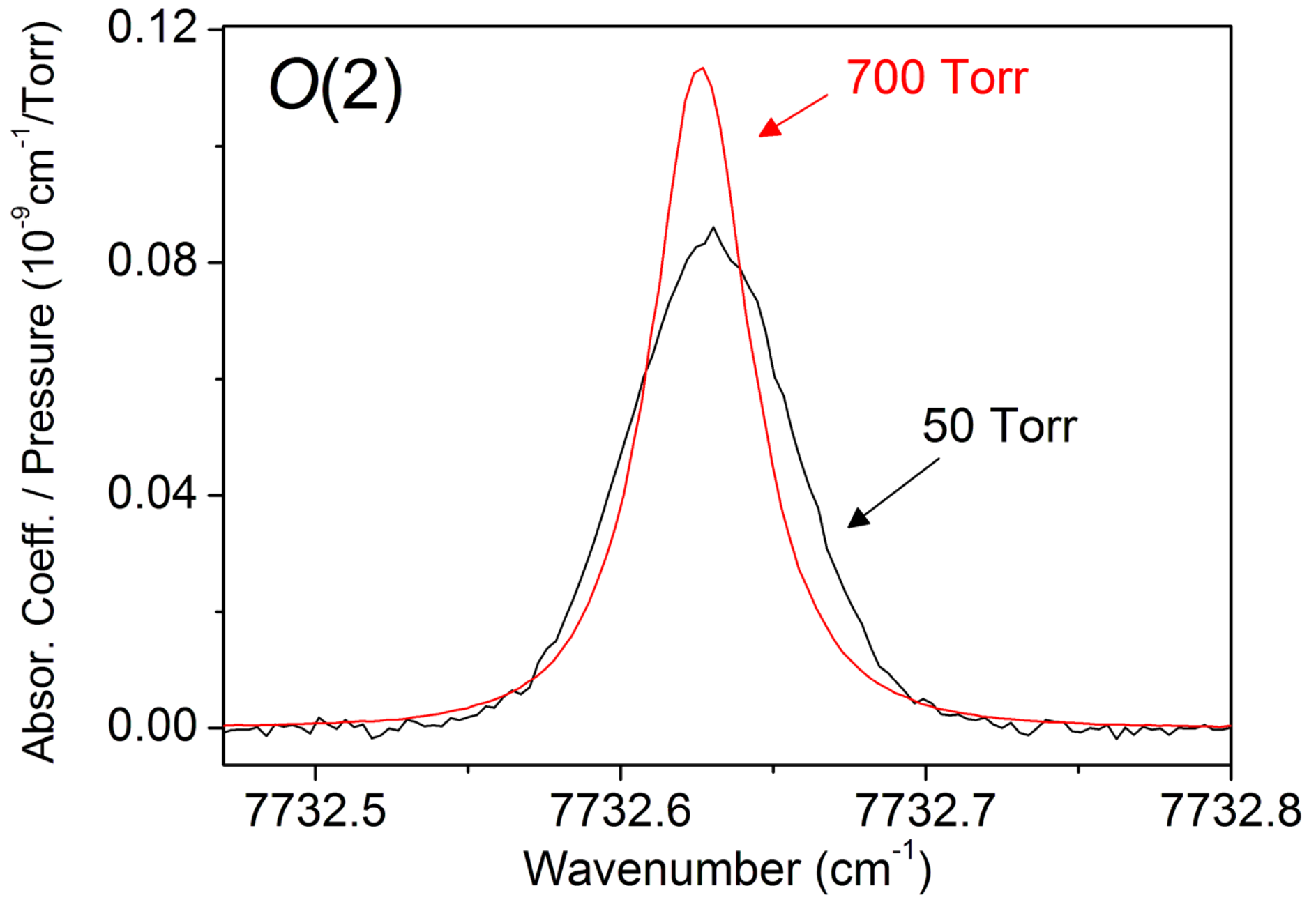
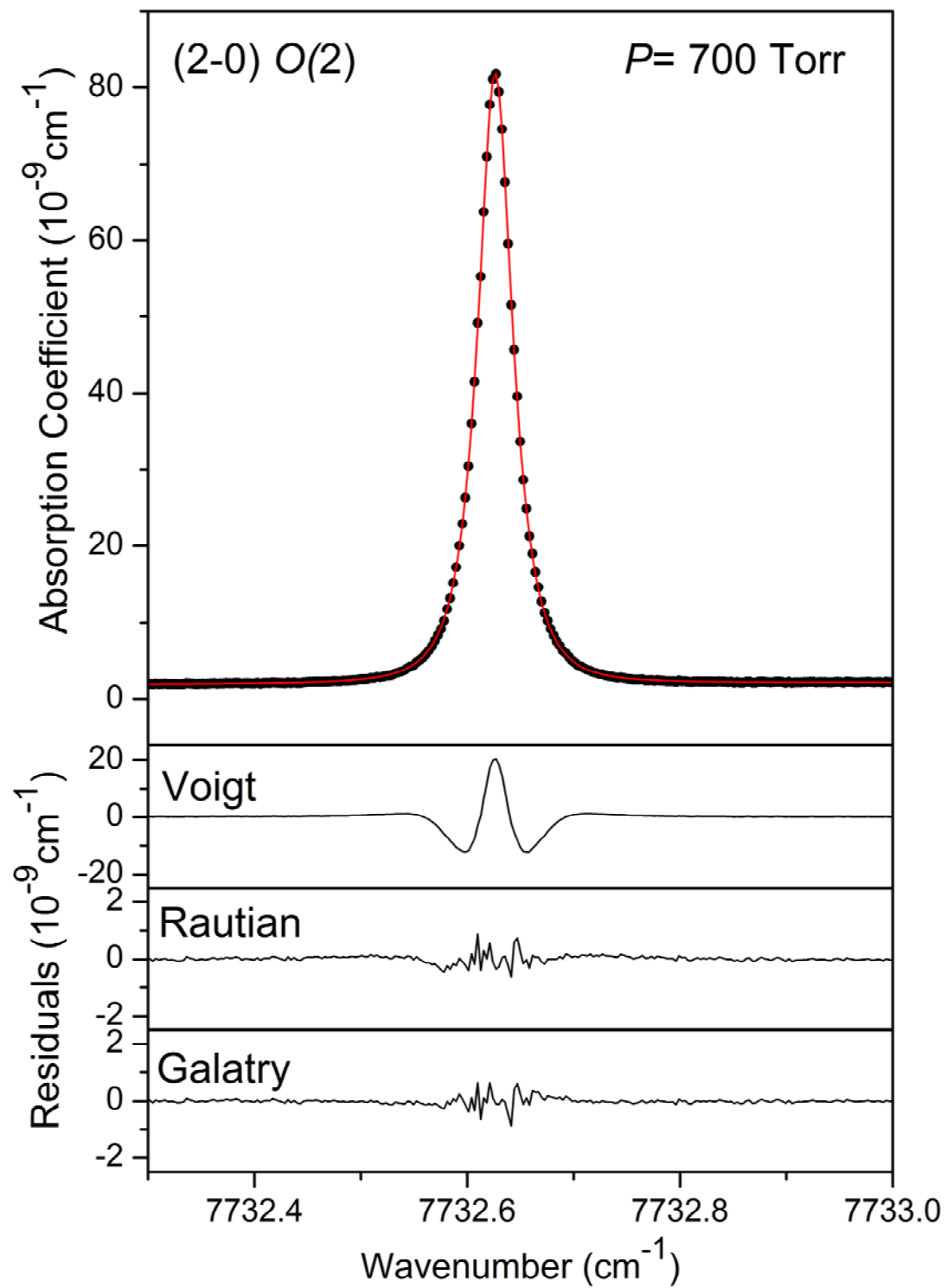
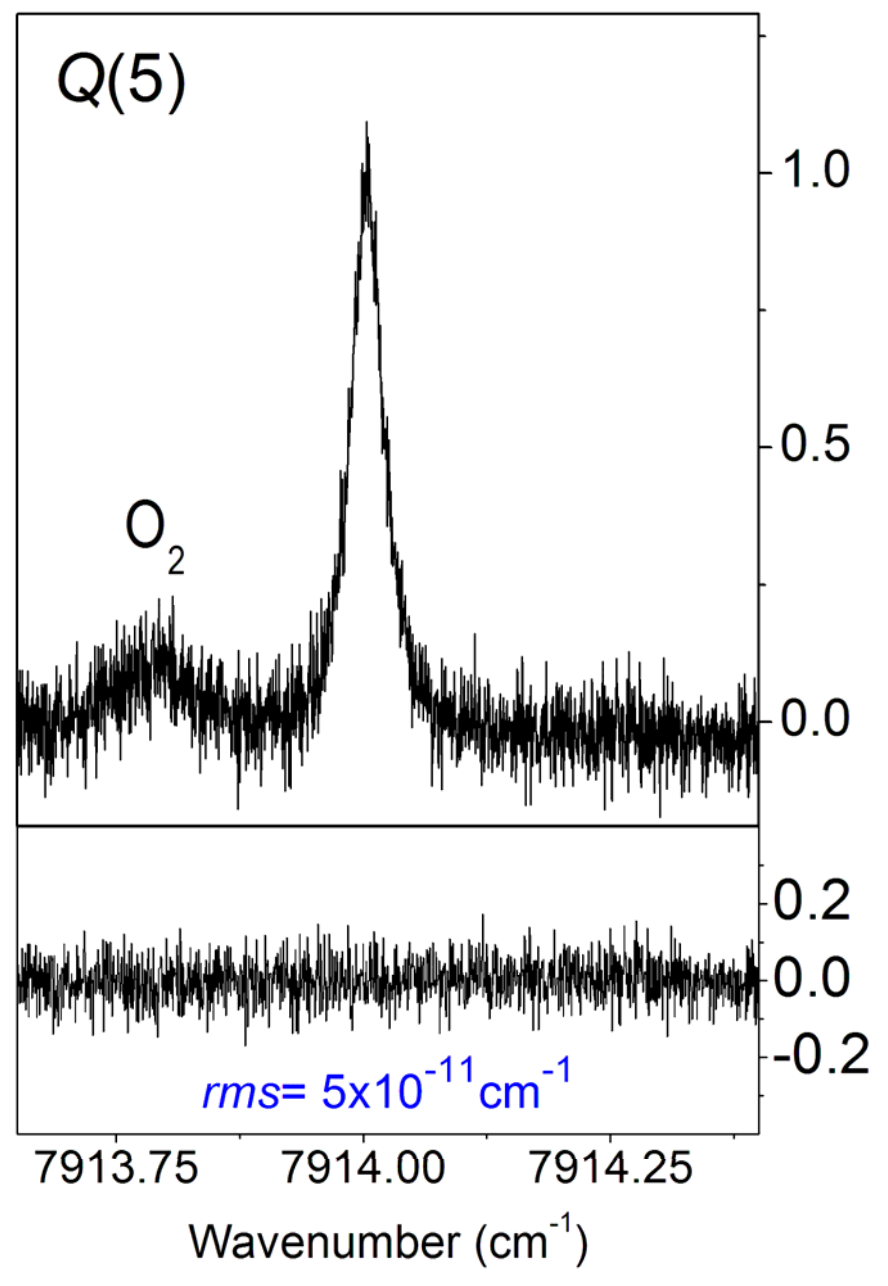
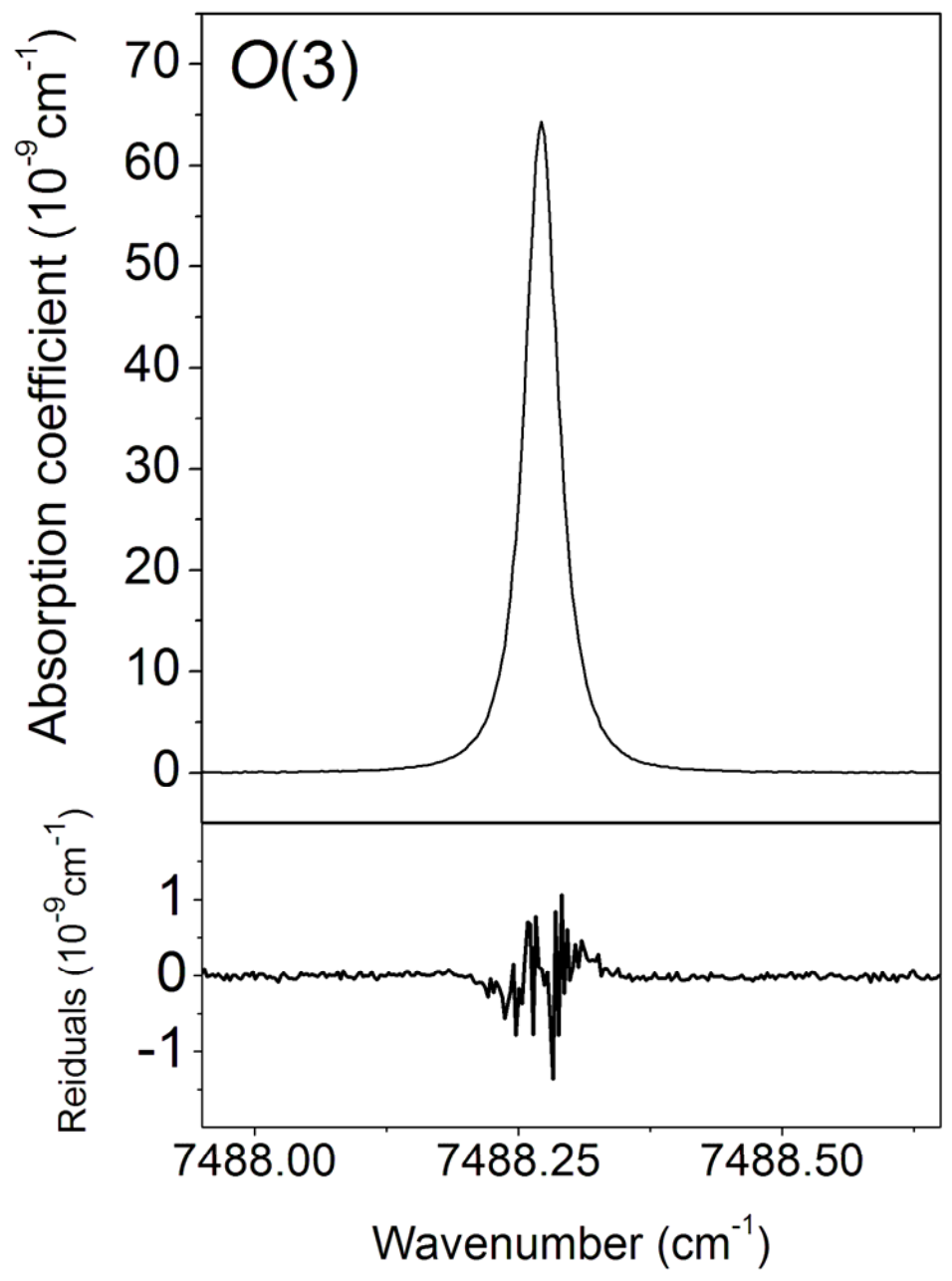


Fig. 2





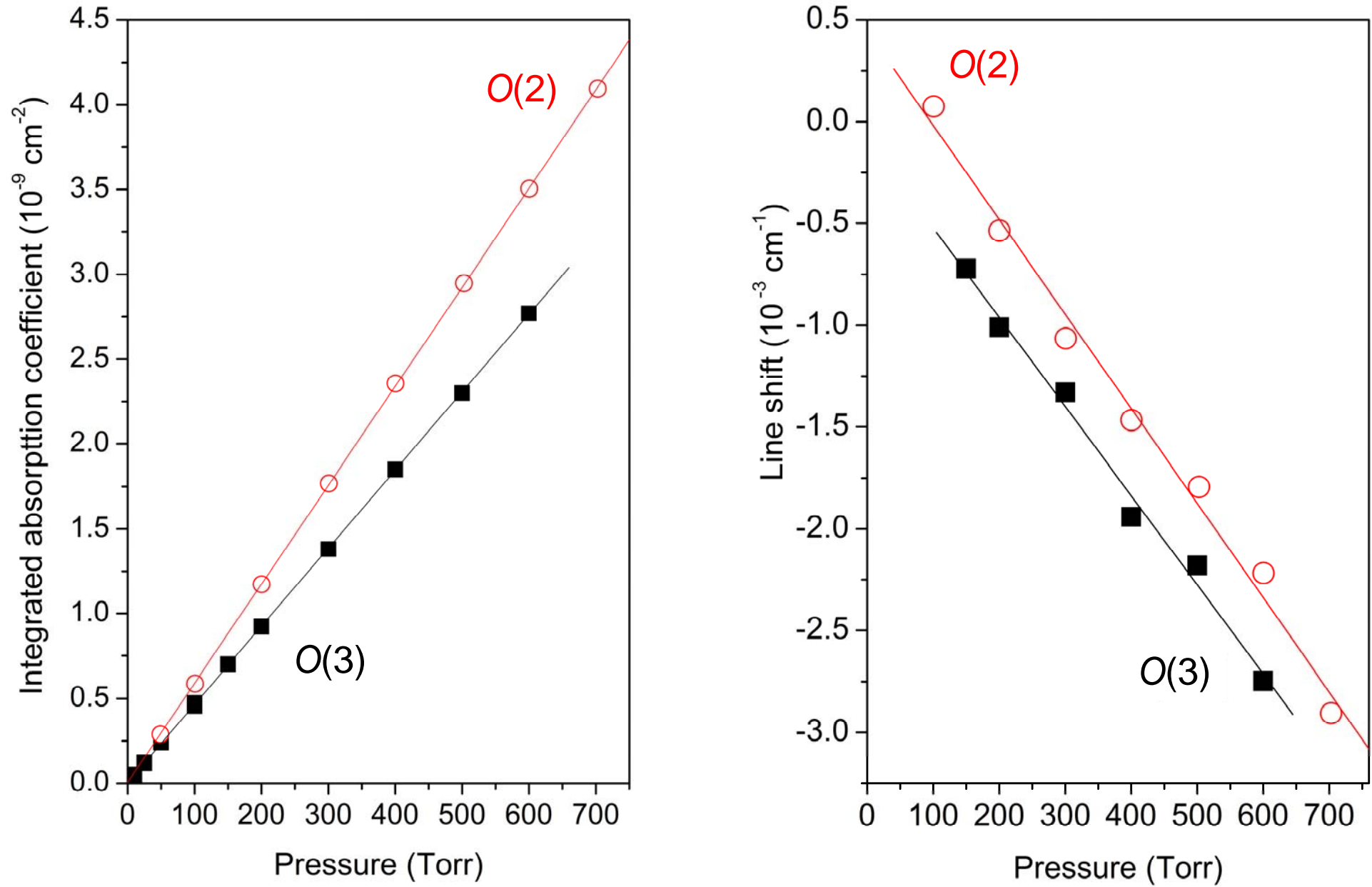


Fig. 4

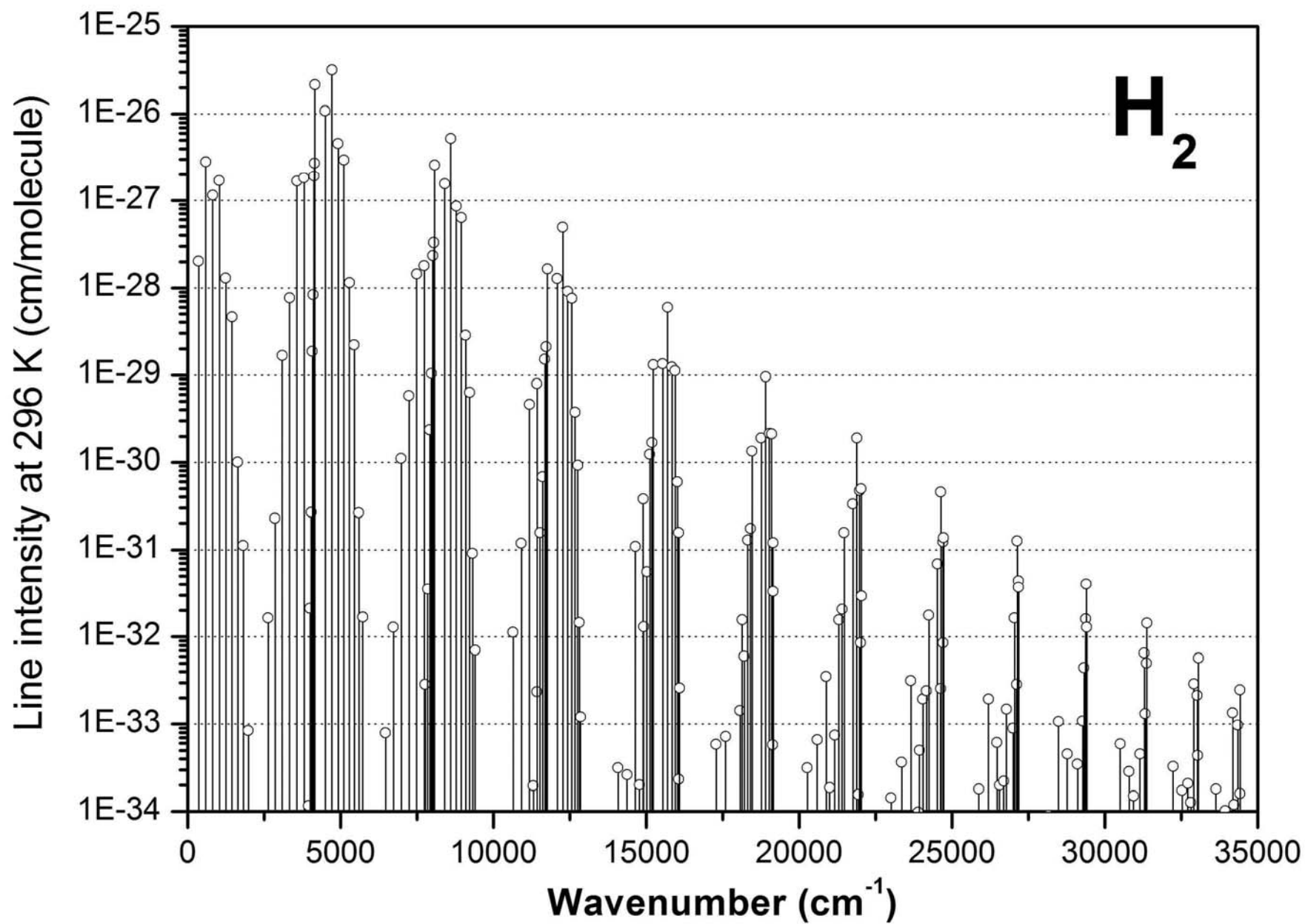


Fig. 5

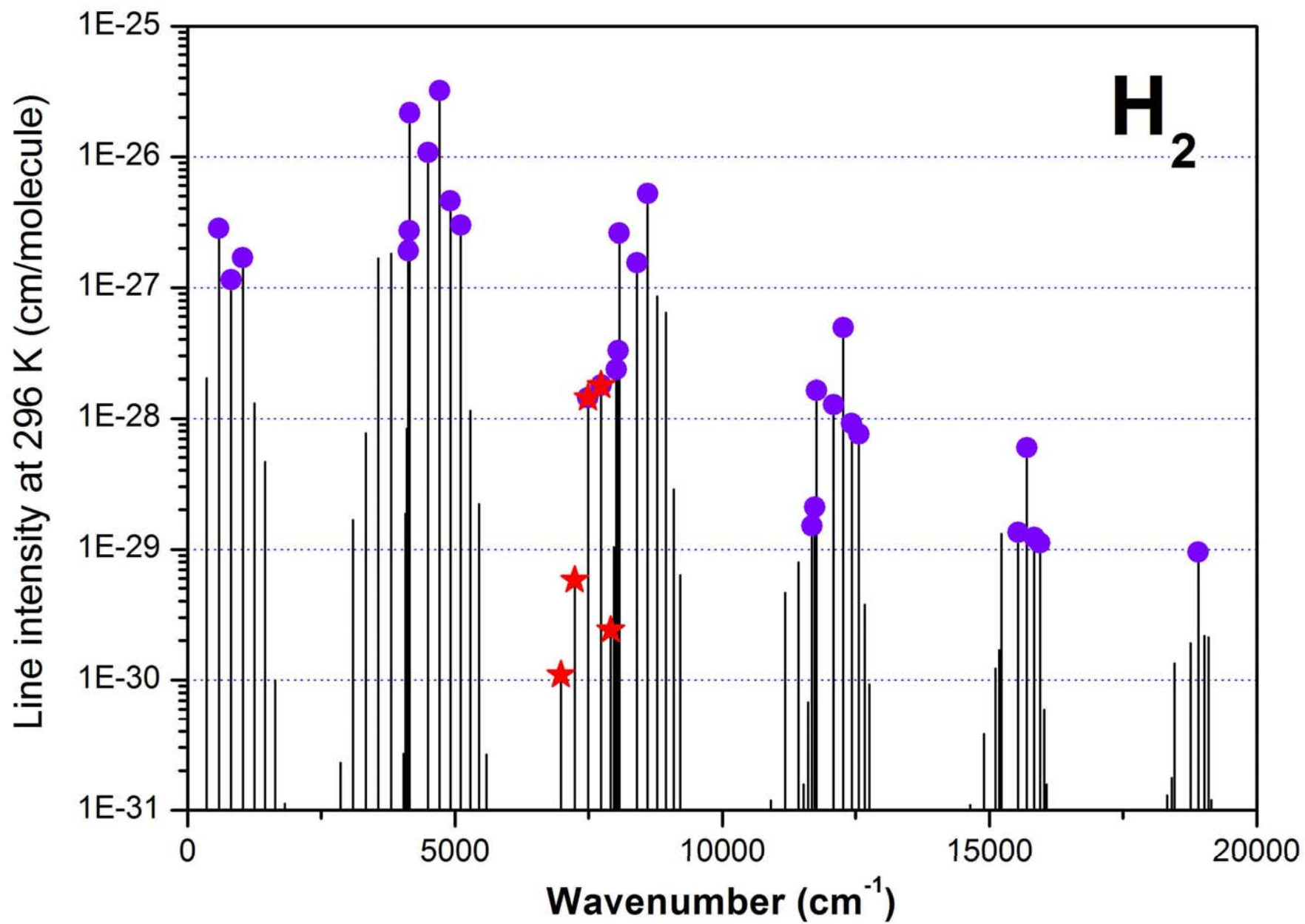


Fig. 6

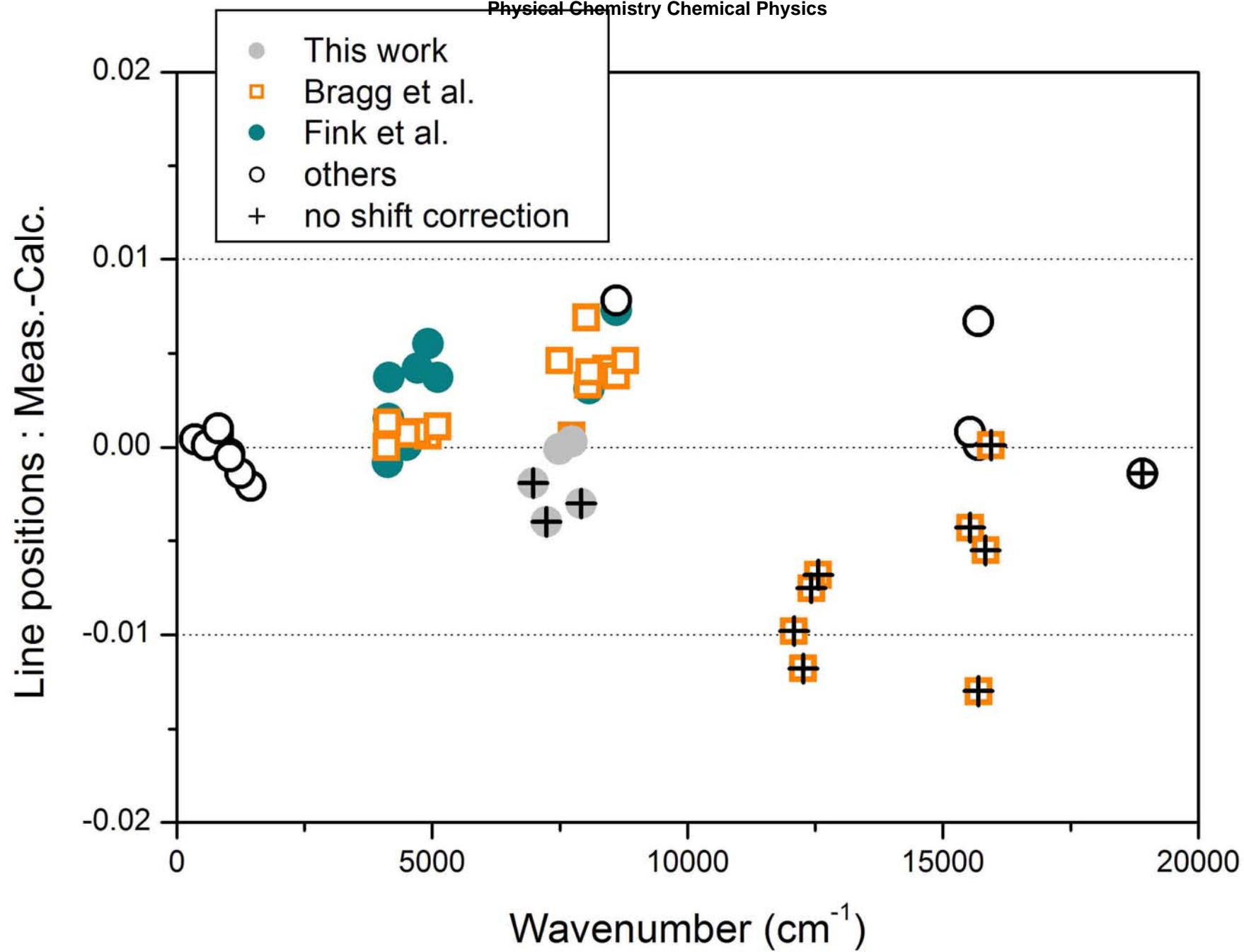
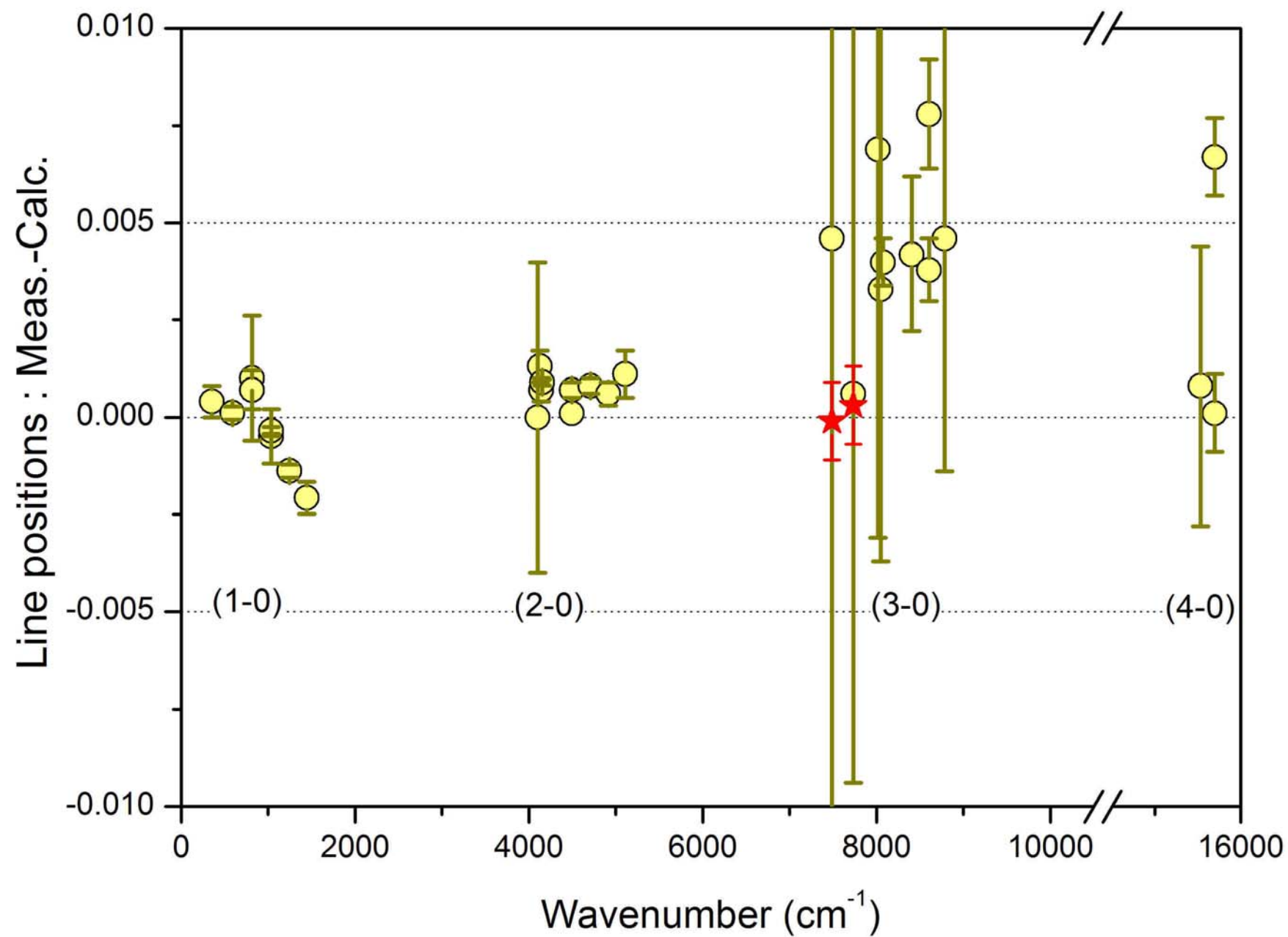


Fig. 7

Fig. 8



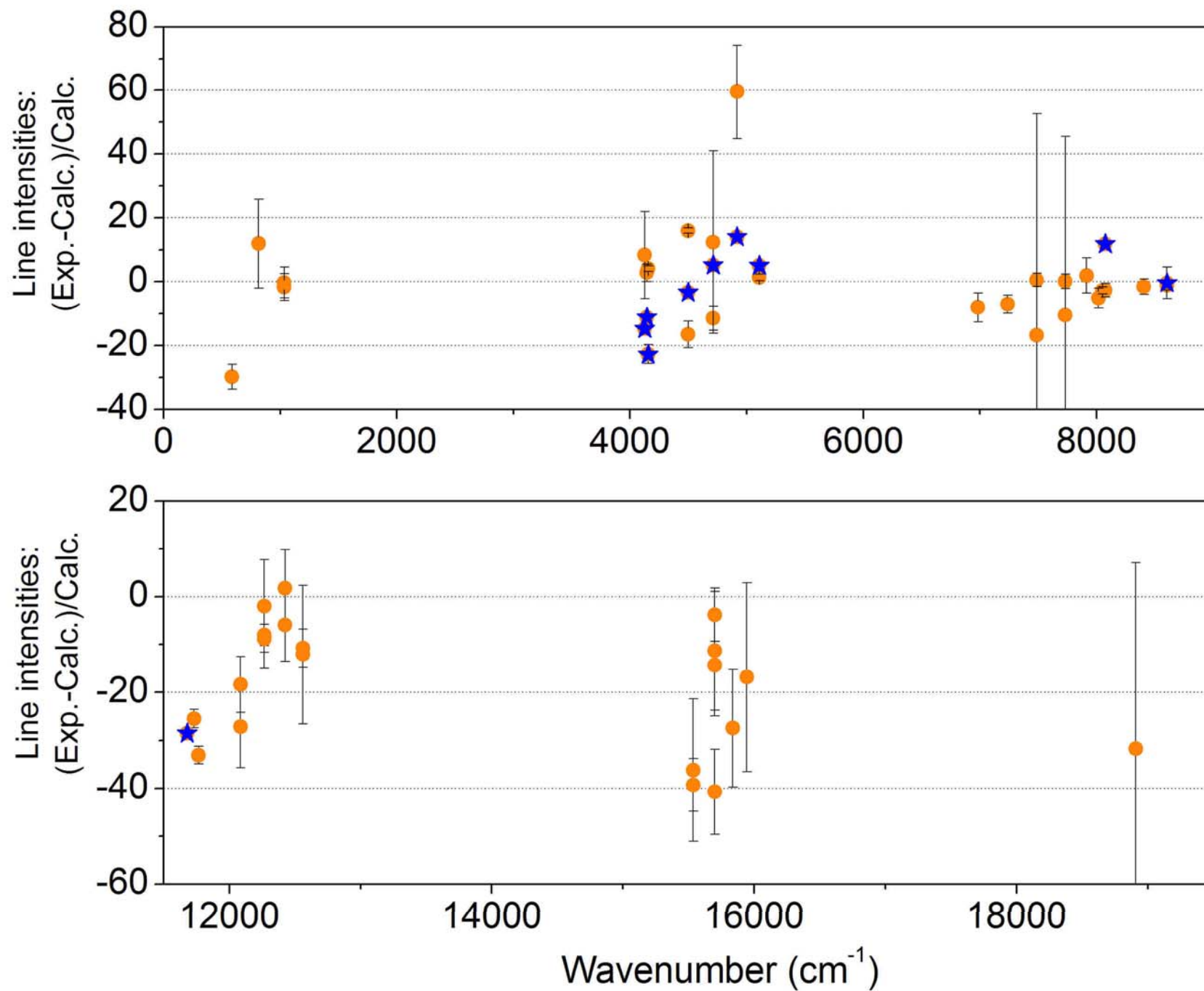


Fig. 9

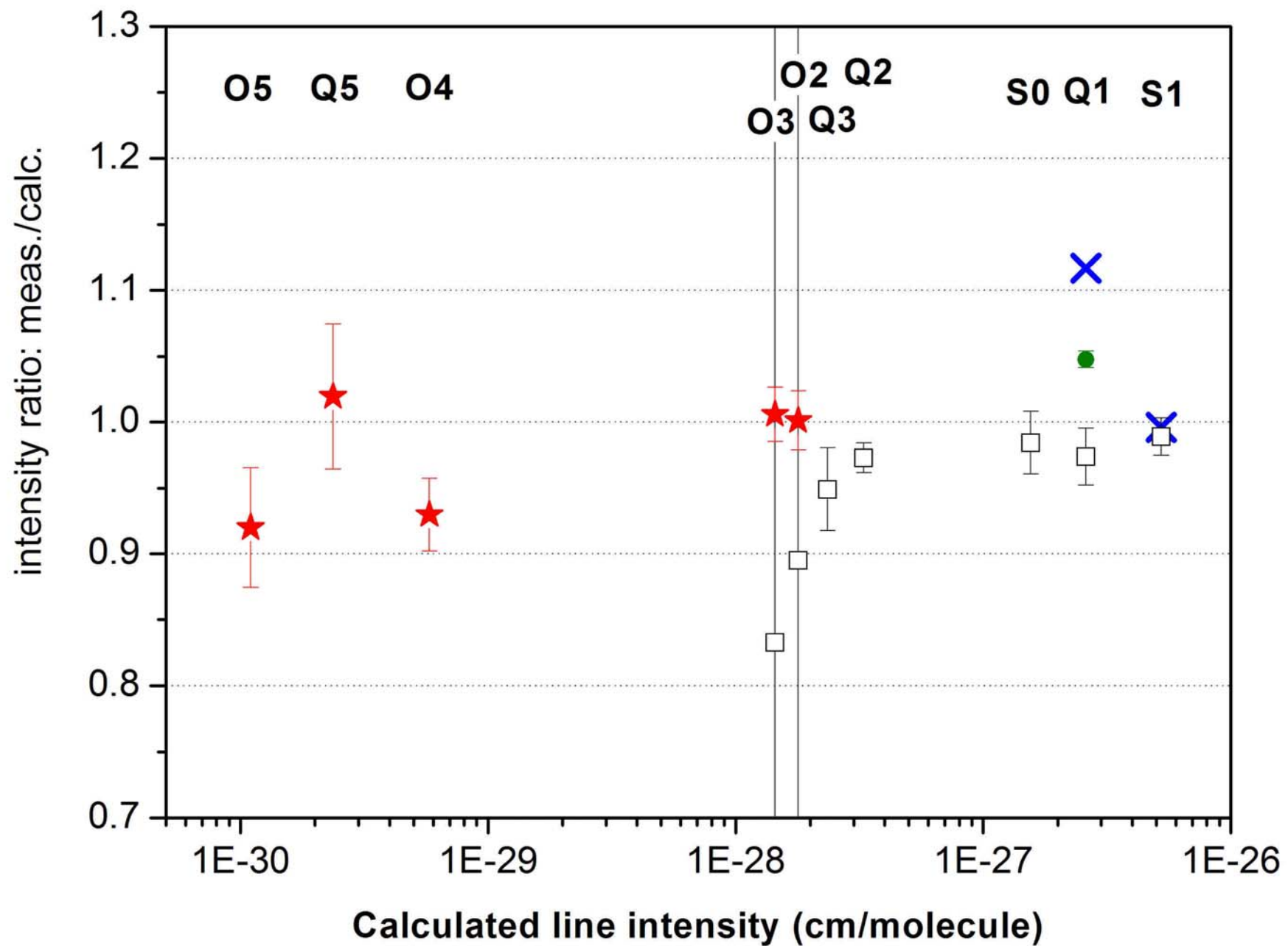


Fig. 10

Supplementary Material attached to the paper: The vibrational absorption spectrum of H₂:

CRDS measurements of the (2-0) band, review of the literature data and accurate ab initio line list up to 35000 cm⁻¹

by

Alain Campargue, Samir Kassi, Krzysztof Pachucki and Jacek Komasa

Calculated list of the H₂ transitions between 0 and 35000 cm⁻¹ at T=296K. The intensity cut off was fixed to 1E-34 cm/molecule.

- (1) Rovibrational assignment
- (2) Line position (cm⁻¹). The number in parenthesis is the uncertainty in the unit of the last quoted digit.
- (3) Transition moment (in atomic unit)
- (4) Einstein coefficient (in Hz)
- (5) Rotational branch
- (6) Lower state energy level (cm⁻¹)
- (7) Boltzmann factor
- (8) Line strength at 296 K in cm/molecule for pure H₂ (100% isotopic abundance)

(5)	(1)	(6)	(2)	(7)	(3)	(8)	(4)
E(J')	(v'',J'') <- (v',J')	PJ(T)	Pos (cm-1)	<v'J' M(R) v''J''>	A(Hz)	Branch	
			Intensity				
0.0000	(0,2) <- (0,0)	0.130361	354.37313 (3)	4.8471E-1	2.940976E-11	S	
118.4869	(0,3) <- (0,1)	0.659573	587.03202 (4)	4.8683E-1	4.758133E-10	S	
354.3732	(0,4) <- (0,2)	0.116421	814.42430 (6)	4.9000E-1	2.752855E-09	S	
705.5189	(0,5) <- (0,3)	0.088718	1034.67068 (8)	4.9422E-1	9.829497E-09	S	
1168.7975	(0,6) <- (0,4)	0.004000	1246.09954 (9)	4.9945E-1	2.641379E-08	S	
1740.1896	(0,7) <- (0,5)	0.000912	1447.28093 (11)	5.0570E-1	5.875555E-08	S	
2414.8970	(0,8) <- (0,6)	0.000014	1637.04600 (13)	5.1292E-1	1.141155E-07	S	
3187.4705	(0,9) <- (0,7)	0.000001	1814.49237 (14)	5.2111E-1	2.000078E-07	S	
4051.9430	(0,0) <- (0,8)	0.000000	1978.97726 (15)	5.3022E-1	3.233529E-07	S	
3187.4705	(1,5) <- (0,7)	0.000001	2626.4512 (8)	1.3113E-1	1.060395E-07	O	
2414.8970	(1,4) <- (0,6)	0.000014	2856.4824 (8)	1.2432E-1	1.496366E-07	O	
1740.1896	(1,3) <- (0,5)	0.000912	3091.2019 (8)	1.1756E-1	2.080232E-07	O	
1168.7975	(1,2) <- (0,4)	0.004000	3329.0410 (9)	1.1084E-1	2.893241E-07	O	
705.5189	(1,1) <- (0,3)	0.088718	3568.2217 (9)	1.0418E-1	4.218437E-07	O	
354.3732	(1,0) <- (0,2)	0.116421	3806.7930 (9)	9.7578E-2	8.525013E-07	O	
			1.818E-27				

(1,8) <- (0,8)	3955.6392 (9)	9.0146E-2	2.226696E-07	Q
4051.9430	0.000000 1.170E-34			
(1,7) <- (0,7)	4000.0551 (9)	8.9670E-2	2.336759E-07	Q
3187.4705	0.000001 2.124E-32			
(1,6) <- (0,6)	4039.4917 (9)	8.9230E-2	2.441314E-07	Q
2414.8970	0.000014 2.686E-31			
(1,5) <- (0,5)	4073.7322 (9)	8.8837E-2	2.542654E-07	Q
1740.1896	0.000912 1.855E-29			
(1,4) <- (0,4)	4102.5820 (9)	8.8498E-2	2.647822E-07	Q
1168.7975	0.004000 8.352E-29			
(1,3) <- (0,3)	4125.8726 (9)	8.8218E-2	2.778835E-07	Q
705.5189	0.088718 1.922E-27			
(1,2) <- (0,2)	4143.4653 (9)	8.8004E-2	3.026584E-07	Q
354.3732	0.116421 2.724E-27			
(1,1) <- (0,1)	4155.2538 (9)	8.7859E-2	4.283675E-07	Q
118.4869	0.659573 2.172E-26			
(1,2) <- (0,0)	4497.8384 (9)	7.8230E-2	2.523430E-07	S
0.0000	0.130361 1.079E-26			
(1,3) <- (0,1)	4712.9046 (9)	7.1950E-2	3.466363E-07	S
118.4869	0.659573 3.188E-26			
(1,4) <- (0,2)	4917.0063 (10)	6.5759E-2	3.976952E-07	S
354.3732	0.116421 4.575E-27			
(1,5) <- (0,3)	5108.4029 (10)	5.9658E-2	4.201949E-07	S
705.5189	0.088718 2.979E-27			
(1,6) <- (0,4)	5285.5912 (10)	5.3642E-2	4.183665E-07	S
1168.7975	0.004000 1.148E-28			
(1,7) <- (0,5)	5447.3360 (10)	4.7705E-2	3.949522E-07	S
1740.1896	0.000912 2.198E-29			
(1,8) <- (0,6)	5592.6852 (10)	4.1835E-2	3.532757E-07	S
2414.8970	0.000014 2.652E-31			
(1,9) <- (0,7)	5720.9703 (10)	3.6019E-2	2.977432E-07	S
3187.4705	0.000001 1.676E-32			
(2,5) <- (0,7)	6466.7267 (16)	7.4880E-3	3.128659E-08	O
3187.4705	0.000001 7.978E-34			
(2,4) <- (0,6)	6725.0006 (16)	8.1916E-3	4.698724E-08	O
2414.8970	0.000014 1.292E-32			
(2,3) <- (0,5)	6982.5124 (17)	8.8635E-3	6.954163E-08	O
1740.1896	0.000912 1.099E-30			
(2,2) <- (0,4)	7237.5634 (17)	9.4917E-3	1.030523E-07	O
1168.7975	0.004000 5.802E-30			
(2,1) <- (0,3)	7488.2754 (17)	1.0065E-2	1.602968E-07	O
705.5189	0.088718 1.443E-28			
(2,0) <- (0,2)	7732.6295 (17)	1.0575E-2	3.462234E-07	O
354.3732	0.116421 1.789E-28			
(2,7) <- (0,7)	7768.1472 (17)	1.2181E-2	1.191109E-07	Q
3187.4705	0.000001 2.870E-33			
(2,6) <- (0,6)	7846.2315 (17)	1.1932E-2	1.206981E-07	Q
2414.8970	0.000014 3.520E-32			
(2,5) <- (0,5)	7914.0076 (17)	1.1719E-2	1.224280E-07	Q
1740.1896	0.000912 2.367E-30			
(2,4) <- (0,4)	7971.1001 (17)	1.1541E-2	1.246865E-07	Q
1168.7975	0.004000 1.042E-29			
(2,3) <- (0,3)	8017.1831 (17)	1.1399E-2	1.285272E-07	Q
705.5189	0.088718 2.355E-28			
(2,2) <- (0,2)	8051.9877 (17)	1.1292E-2	1.380999E-07	Q
354.3732	0.116421 3.291E-28			
(2,1) <- (0,1)	8075.3074 (17)	1.1221E-2	1.936902E-07	Q
118.4869	0.659573 2.600E-27			
(2,2) <- (0,0)	8406.3608 (18)	1.1637E-2	1.273300E-07	S
0.0000	0.130361 1.559E-27			

(2,3) <- (0,1)	8604.2152 (18)	1.1819E-2	1.897171E-07	S
118.4869	0.659573 5.234E-27			
(2,4) <- (0,2)	8785.5244 (18)	1.1912E-2	2.376675E-07	S
354.3732	0.116421 8.564E-28			
(2,5) <- (0,3)	8948.6783 (18)	1.1917E-2	2.765727E-07	S
705.5189	0.088718 6.391E-28			
(2,6) <- (0,4)	9092.3310 (18)	1.1835E-2	3.067375E-07	S
1168.7975	0.004000 2.845E-29			
(2,7) <- (0,5)	9215.4281 (18)	1.1669E-2	3.274350E-07	S
1740.1896	0.000912 6.366E-30			
(2,8) <- (0,6)	9317.2177 (18)	1.1422E-2	3.379724E-07	S
2414.8970	0.000014 9.142E-32			
(2,9) <- (0,7)	9397.2457 (18)	1.1100E-2	3.380900E-07	S
3187.4705	0.000001 7.051E-33			
(3,3) <- (0,5)	10643.8922 (24)	4.7818E-4	1.665982E-09	O
1740.1896	0.000912 1.133E-32			
(3,2) <- (0,4)	10915.8996 (24)	7.3464E-4	4.817869E-09	O
1168.7975	0.004000 1.193E-31			
(3,1) <- (0,3)	11177.9689 (24)	9.8951E-4	1.148170E-08	O
705.5189	0.088718 4.637E-30			
(3,7) <- (0,7)	11307.9726 (24)	1.8142E-3	1.726957E-08	Q
3187.4705	0.000001 1.964E-34			
(3,6) <- (0,6)	11424.2163 (24)	1.7595E-3	1.717436E-08	Q
2414.8970	0.000014 2.363E-33			
(3,0) <- (0,2)	11428.0177 (25)	1.2399E-3	3.355810E-08	O
354.3732	0.116421 7.941E-30			
(3,5) <- (0,5)	11525.0786 (24)	1.7129E-3	1.713274E-08	Q
1740.1896	0.000912 1.562E-31			
(3,4) <- (0,4)	11610.0178 (25)	1.6742E-3	1.720029E-08	Q
1168.7975	0.004000 6.774E-31			
(3,3) <- (0,3)	11678.5629 (25)	1.6434E-3	1.752186E-08	Q
705.5189	0.088718 1.513E-29			
(3,2) <- (0,2)	11730.3239 (25)	1.6202E-3	1.865673E-08	Q
354.3732	0.116421 2.095E-29			
(3,1) <- (0,1)	11765.0009 (25)	1.6048E-3	2.600597E-08	Q
118.4869	0.659573 1.645E-28			
(3,2) <- (0,0)	12084.6970 (25)	1.9322E-3	2.155403E-08	S
0.0000	0.130361 1.277E-28			
(3,3) <- (0,1)	12265.5949 (25)	2.1333E-3	3.638613E-08	S
118.4869	0.659573 4.940E-28			
(3,4) <- (0,2)	12424.4421 (25)	2.3152E-3	5.078207E-08	S
354.3732	0.116421 9.150E-29			
(3,5) <- (0,3)	12559.7492 (25)	2.4760E-3	6.502856E-08	S
705.5189	0.088718 7.628E-29			
(3,6) <- (0,4)	12670.3158 (25)	2.6143E-3	7.865514E-08	S
1168.7975	0.004000 3.757E-30			
(3,7) <- (0,5)	12755.2535 (25)	2.7292E-3	9.099591E-08	S
1740.1896	0.000912 9.235E-31			
(3,8) <- (0,6)	12813.9923 (25)	2.8203E-3	1.013814E-07	S
2414.8970	0.000014 1.450E-32			
(3,9) <- (0,7)	12846.2712 (25)	2.8877E-3	1.092460E-07	S
3187.4705	0.000001 1.219E-33			
(4,3) <- (0,5)	14078.0983 (31)	5.2561E-5	8.147604E-11	O
1740.1896	0.000912 3.168E-34			
(4,2) <- (0,4)	14366.9458 (31)	2.2902E-5	1.849187E-11	O
1168.7975	0.004000 2.642E-34			
(4,1) <- (0,3)	14640.2910 (31)	1.0153E-4	4.658524E-10	O
705.5189	0.088718 1.097E-31			
(4,6) <- (0,6)	14775.4941 (31)	3.4904E-4	2.445790E-09	Q
2414.8970	0.000014 2.012E-34			

(4,0) <- (0,2)	14895.9925	(31)	1.8261E-4	2.739046E-09	O
354.3732	0.116421	3.815E-31			
(4,5) <- (0,5)	14909.2792	(31)	3.3676E-4	2.399154E-09	Q
1740.1896	0.000912	1.307E-32			
(4,4) <- (0,4)	15021.9052	(31)	3.2654E-4	2.372688E-09	Q
1168.7975	0.004000	5.582E-32			
(4,3) <- (0,3)	15112.7690	(31)	3.1837E-4	2.386405E-09	Q
705.5189	0.088718	1.230E-30			
(4,2) <- (0,2)	15181.3701	(31)	3.1223E-4	2.515584E-09	Q
354.3732	0.116421	1.687E-30			
(4,1) <- (0,1)	15227.3230	(32)	3.0814E-4	3.482288E-09	Q
118.4869	0.659573	1.315E-29			
(4,2) <- (0,0)	15535.7432	(32)	4.3098E-4	3.765329E-09	S
0.0000	0.130361	1.350E-29			
(4,3) <- (0,1)	15699.8010	(32)	5.1170E-4	7.192533E-09	S
118.4869	0.659573	5.960E-29			
(4,4) <- (0,2)	15836.3295	(32)	5.8946E-4	1.107402E-08	S
354.3732	0.116421	1.228E-29			
(4,5) <- (0,3)	15943.9499	(32)	6.6317E-4	1.537852E-08	S
705.5189	0.088718	1.119E-29			
(4,6) <- (0,4)	16021.5936	(32)	7.3193E-4	1.993137E-08	S
1168.7975	0.004000	5.954E-31			
(4,7) <- (0,5)	16068.5214	(32)	7.9497E-4	2.449544E-08	S
1740.1896	0.000912	1.566E-31			
(4,9) <- (0,7)	16068.9109	(31)	9.0185E-4	3.263016E-08	S
3187.4705	0.000001	2.328E-34			
(4,8) <- (0,6)	16084.3247	(31)	8.5174E-4	2.881139E-08	S
2414.8970	0.000014	2.615E-33			
(5,3) <- (0,5)	17285.8147	(37)	5.2629E-5	2.279726E-10	O
1740.1896	0.000912	5.879E-34			
(5,2) <- (0,4)	17591.5461	(37)	2.7877E-5	7.540858E-11	O
1168.7975	0.004000	7.187E-34			
(5,5) <- (0,5)	18066.8060	(37)	8.3701E-5	3.872579E-10	Q
1740.1896	0.000912	1.437E-33			
(5,0) <- (0,2)	18137.5564	(37)	2.7544E-5	1.667845E-10	O
354.3732	0.116421	1.567E-32			
(5,4) <- (0,4)	18207.2310	(37)	8.0215E-5	3.745179E-10	Q
1168.7975	0.004000	5.998E-33			
(5,3) <- (0,3)	18320.4854	(37)	7.7422E-5	3.694737E-10	Q
705.5189	0.088718	1.296E-31			
(5,2) <- (0,2)	18405.9704	(37)	7.5323E-5	3.835099E-10	Q
354.3732	0.116421	1.749E-31			
(5,1) <- (0,1)	18463.2234	(37)	7.3920E-5	5.251980E-10	Q
118.4869	0.659573	1.349E-30			
(5,2) <- (0,0)	18760.3435	(38)	1.2190E-4	7.734007E-10	S
0.0000	0.130361	1.901E-30			
(5,3) <- (0,1)	18907.5174	(38)	1.5481E-4	1.667898E-09	S
118.4869	0.659573	9.530E-30			
(5,4) <- (0,2)	19021.6553	(38)	1.8769E-4	2.807054E-09	S
354.3732	0.116421	2.158E-30			
(5,5) <- (0,3)	19101.4767	(37)	2.2004E-4	4.178545E-09	S
705.5189	0.088718	2.119E-30			
(5,8) <- (0,6)	19127.2227	(37)	3.0977E-4	9.062850E-09	S
2414.8970	0.000014	5.817E-34			
(5,6) <- (0,4)	19146.0288	(37)	2.5142E-4	5.731584E-09	S
1168.7975	0.004000	1.199E-31			
(5,7) <- (0,5)	19154.7014	(37)	2.8144E-4	7.390092E-09	S
1740.1896	0.000912	3.326E-32			
(6,3) <- (0,5)	20265.3607	(42)	3.0434E-5	1.688324E-10	O
1740.1896	0.000912	3.168E-34			

(6,2) <- (0,4)	20588.2094	(42)	2.1079E-5	9.467054E-11	O
1168.7975	0.004000	6.587E-34			
(6,1) <- (0,3)	20884.3046	(42)	1.0655E-5	3.030803E-11	O
705.5189	0.088718	3.507E-33			
(6,5) <- (0,5)	20995.3964	(42)	2.4067E-5	6.785544E-11	Q
1740.1896	0.000912	1.864E-34			
(6,4) <- (0,4)	21164.0583	(42)	2.2645E-5	6.334199E-11	Q
1168.7975	0.004000	7.508E-34			
(6,3) <- (0,3)	21300.0314	(42)	2.1506E-5	6.056053E-11	Q
705.5189	0.088718	1.572E-32			
(6,2) <- (0,2)	21402.6337	(42)	2.0649E-5	6.127446E-11	Q
354.3732	0.116421	2.067E-32			
(6,1) <- (0,1)	21471.3366	(43)	2.0077E-5	8.240355E-11	Q
118.4869	0.659573	1.565E-31			
(6,2) <- (0,0)	21757.0068	(43)	4.0822E-5	1.819732E-10	S
0.0000	0.130361	3.326E-31			
(6,3) <- (0,1)	21887.0634	(43)	5.5521E-5	4.458820E-10	S
118.4869	0.659573	1.901E-30			
(6,8) <- (0,6)	21938.9866	(42)	1.3033E-4	3.184773E-09	S
2414.8970	0.000014	1.554E-34			
(6,4) <- (0,2)	21978.4826	(43)	7.0584E-5	8.175825E-10	S
354.3732	0.116421	4.707E-31			
(6,7) <- (0,5)	22010.6553	(42)	1.1585E-4	2.508741E-09	S
1740.1896	0.000912	8.550E-33			
(6,5) <- (0,3)	22030.0671	(42)	8.5797E-5	1.296321E-09	S
705.5189	0.088718	4.942E-31			
(6,6) <- (0,4)	22040.9602	(42)	1.0095E-4	1.868295E-09	S
1168.7975	0.004000	2.949E-32			
(7,3) <- (0,5)	23012.2739	(46)	1.6969E-5	9.910340E-11	O
1740.1896	0.000912	1.442E-34			
(7,2) <- (0,4)	23352.7060	(46)	1.2969E-5	6.727787E-11	O
1168.7975	0.004000	3.639E-34			
(7,1) <- (0,3)	23660.5543	(46)	8.4003E-6	3.516089E-11	O
705.5189	0.088718	3.170E-33			
(7,0) <- (0,2)	23933.5421	(47)	3.2481E-6	9.278962E-12	O
354.3732	0.116421	5.006E-34			
(7,3) <- (0,3)	24046.9446	(46)	6.2981E-6	9.525582E-12	Q
705.5189	0.088718	1.940E-33			
(7,2) <- (0,2)	24167.1303	(47)	5.9020E-6	9.188596E-12	Q
354.3732	0.116421	2.431E-33			
(7,1) <- (0,1)	24247.5864	(47)	5.6373E-6	1.193274E-11	Q
118.4869	0.659573	1.777E-32			
(7,2) <- (0,0)	24521.5035	(47)	1.5529E-5	4.789186E-11	S
0.0000	0.130361	6.890E-32			
(7,7) <- (0,5)	24630.1107	(46)	5.3772E-5	9.482954E-10	S
1740.1896	0.000912	2.581E-33			
(7,3) <- (0,1)	24633.9766	(47)	2.2719E-5	1.348434E-10	S
118.4869	0.659573	4.539E-31			
(7,6) <- (0,4)	24700.7121	(46)	4.5864E-5	6.816533E-10	S
1168.7975	0.004000	8.567E-33			
(7,4) <- (0,2)	24702.0338	(47)	3.0238E-5	2.690965E-10	S
354.3732	0.116421	1.227E-31			
(7,5) <- (0,3)	24724.5412	(46)	3.7987E-5	4.524781E-10	S
705.5189	0.088718	1.370E-31			
(8,2) <- (0,4)	25877.4995	(49)	7.8560E-6	4.124901E-11	O
1168.7975	0.004000	1.817E-34			
(8,1) <- (0,3)	26197.5981	(49)	5.6416E-6	2.639094E-11	O
705.5189	0.088718	1.940E-33			
(8,0) <- (0,2)	26476.7175	(50)	3.0948E-6	1.395701E-11	O
354.3732	0.116421	6.153E-34			

(8,3) <- (0,3) 26553.3932 (49)	1.7392E-6	1.192538E-12	Q
705.5189 0.088718 1.992E-34			
(8,2) <- (0,2) 26691.9238 (50)	1.5372E-6	1.024482E-12	Q
354.3732 0.116421 2.222E-34			
(8,1) <- (0,1) 26784.6301 (50)	1.4024E-6	1.214556E-12	Q
118.4869 0.659573 1.482E-33			
(8,7) <- (0,5) 27002.9037 (48)	2.7566E-5	3.947349E-10	S
1740.1896 0.000912 8.938E-34			
(8,2) <- (0,0) 27046.2970 (50)	6.5450E-6	1.388643E-11	S
0.0000 0.130361 1.642E-32			
(8,6) <- (0,4) 27115.8975 (49)	2.3075E-5	2.750811E-10	S
1168.7975 0.004000 2.869E-33			
(8,3) <- (0,1) 27140.4253 (50)	1.0363E-5	4.554093E-11	S
118.4869 0.659573 1.263E-31			
(8,5) <- (0,3) 27176.1508 (49)	1.8677E-5	1.754814E-10	S
705.5189 0.088718 4.397E-32			
(8,4) <- (0,2) 27184.0758 (49)	1.4423E-5	9.880794E-11	S
354.3732 0.116421 3.719E-32			
(9,1) <- (0,3) 28484.0451 (51)	3.7121E-6	1.736188E-11	O
705.5189 0.088718 1.080E-33			
(9,0) <- (0,2) 28769.6672 (51)	2.3429E-6	1.211671E-11	O
354.3732 0.116421 4.524E-34			
(9,7) <- (0,5) 29113.8774 (49)	1.5372E-5	1.788315E-10	S
1740.1896 0.000912 3.484E-34			
(9,6) <- (0,4) 29272.4119 (50)	1.2656E-5	1.213335E-10	S
1168.7975 0.004000 1.086E-33			
(9,2) <- (0,0) 29319.7424 (51)	3.0072E-6	4.388857E-12	S
0.0000 0.130361 4.417E-33			
(9,5) <- (0,3) 29371.6485 (50)	1.0036E-5	7.472541E-11	S
705.5189 0.088718 1.603E-32			
(9,3) <- (0,1) 29394.3770 (51)	5.1867E-6	1.700093E-11	S
118.4869 0.659573 4.019E-32			
(9,4) <- (0,2) 29412.0461 (51)	7.5376E-6	4.001537E-11	S
354.3732 0.116421 1.287E-32			
(10,1) <- (0,3) 30503.3511 (51)	2.4793E-6	1.090806E-11	O
705.5189 0.088718 5.916E-34			
(10,0) <- (0,2) 30796.0178 (51)	1.6872E-6	8.831125E-12	O
354.3732 0.116421 2.878E-34			
(10,7) <- (0,5) 30941.2209 (48)	9.2043E-6	8.693029E-11	S
1740.1896 0.000912 1.499E-34			
(10,6) <- (0,4) 31149.9497 (49)	7.4722E-6	5.771110E-11	S
1168.7975 0.004000 4.561E-34			
(10,5) <- (0,3) 31291.9341 (50)	5.8206E-6	3.449659E-11	S
705.5189 0.088718 6.519E-33			
(10,2) <- (0,0) 31324.9505 (51)	1.4911E-6	1.502014E-12	S
0.0000 0.130361 1.324E-33			
(10,4) <- (0,2) 31367.7960 (50)	4.2640E-6	1.766817E-11	S
354.3732 0.116421 4.994E-33			
(10,3) <- (0,1) 31378.4126 (51)	2.8168E-6	6.950790E-12	S
118.4869 0.659573 1.442E-32			
(11,1) <- (0,3) 32232.2305 (48)	1.6955E-6	6.720634E-12	O
705.5189 0.088718 3.264E-34			
(11,0) <- (0,2) 32532.7252 (48)	1.2078E-6	5.953271E-12	O
354.3732 0.116421 1.738E-34			
(11,6) <- (0,4) 32719.7041 (45)	4.6853E-6	2.901321E-11	S
1168.7975 0.004000 2.078E-34			
(11,1) <- (0,1) 32819.2626 (48)	3.0267E-7	1.562589E-13	Q
118.4869 0.659573 1.270E-34			
(11,5) <- (0,3) 32910.0105 (46)	3.5979E-6	1.695942E-11	S
705.5189 0.088718 2.897E-33			

(11,4)	<-	(0,2)	33025.7288	(47)	2.5810E-6	8.374549E-12	S
354.3732			0.116421	2.136E-33			
(11,2)	<-	(0,0)	33038.1431	(48)	7.9302E-7	5.544606E-13	S
0.0000			0.130361	4.394E-34			
(11,3)	<-	(0,1)	33067.9934	(48)	1.6437E-6	3.076394E-12	S
118.4869			0.659573	5.746E-33			
(12,1)	<-	(0,3)	33638.3294	(42)	1.1814E-6	4.039399E-12	O
705.5189			0.088718	1.801E-34			
(12,0)	<-	(0,2)	33947.8009	(42)	8.6653E-7	3.791653E-12	O
354.3732			0.116421	1.017E-34			
(12,5)	<-	(0,3)	34187.6897	(38)	2.3239E-6	8.560171E-12	S
705.5189			0.088718	1.355E-33			
(12,1)	<-	(0,1)	34225.3614	(42)	2.7509E-7	1.592010E-13	Q
118.4869			0.659573	1.190E-34			
(12,4)	<-	(0,2)	34349.9117	(40)	1.6431E-6	4.131090E-12	S
354.3732			0.116421	9.738E-34			
(12,2)	<-	(0,0)	34426.2179	(42)	4.4932E-7	2.186718E-13	S
0.0000			0.130361	1.596E-34			
(12,3)	<-	(0,1)	34428.8463	(41)	1.0161E-6	1.438267E-12	S
118.4869			0.659573	2.478E-33			